reactions

MDPI

Article

Study of the Degradation Kinetics and Photocatalytic Mineralization of the Dye 2-(4-Amino-2-Nitrophenyl)-1,3-Benzothiazole: Effect of TiO_2 Dosage, pH, and Aeration on COD

Luis Américo Carrasco-Venegas [1,*], Juan Taumaturgo Medina-Collana [2,*], Luz Genara Castañeda-Pérez [3], Daril Giovanni Martínez-Hilario [2], Cesar Gutiérrez-Cuba [2], Héctor Ricardo Cuba-Torre [2], Rodolfo Paz-Salazar [2], Flor Ortega-Blas [2] and Salvador Trujillo Pérez [2]

[1] Bioenergy Research Center, National University of Callao, Callao 15001, Peru
[2] Faculty of Chemical Engineering, National University of Callao, Callao 15001, Peru; dgmartinezh@unac.edu.pe (D.G.M.-H.); cgutierrezc@unac.edu.pe (C.G.-C.); hrcubat@unac.edu.pe (H.R.C.-T.); rpazs@unac.edu.pe (R.P.-S.); fmortegab@unac.edu.pe (F.O.-B.); satrujillop@unac.edu.pe (S.T.P.)
[3] Faculty of Natural Sciences and Mathematics, Universidad Nacional Federico Villareal, Lima 15001, Peru; lcastaneda@unfv.edu.pe
* Correspondence: lacarrascov@unac.edu.pe (L.A.C.-V.); jtmedinac@unac.edu.pe (J.T.M.-C.)

Abstract

The objective of this study was to evaluate the solar photocatalytic degradation of the disperse textile dye 2-(4-amino-2-nitrophenyl)-1,3-benzothiazole using titanium dioxide nanoparticles (TiO_2 P25) under a mean solar irradiance of 492 ± 58 W/m^2, evaluating the effects of pH, photocatalyst concentration, and continuous aeration on process efficiency. The degradation of the dye was determined by monitoring its concentration by UV–Visible spectrophotometry, while the mineralization was evaluated by chemical oxygen demand (COD). Likewise, kinetic behavior was analyzed using pseudo-first-order and pseudo-second-order models. The results showed that the degradation efficiency increased with the concentration of TiO_2, reaching the highest yield with 400 ppm of TiO_2 and continuous aeration, which confirms that both variables are determining operating factors for maximizing photocatalytic efficiency. pH exerted a significant influence on the activity of the system, obtaining the highest degradation efficiencies and the greatest reductions in COD under slightly alkaline conditions (pH 8–9), a behavior attributed to the greater colloidal stability of TiO_2 and the modification of its surface properties with respect to its point of zero charge (pHpzc ≈ 6.2). The pseudo-second-order model generally provided an adequate empirical description of the experimental data; however, the best-fitting model varied depending on the experimental condition. The simultaneous decrease in the concentration of the dye and the COD confirmed that the treatment produced not only the decolorization of the solution, but also the progressive oxidation of the organic matter. Integrating kinetic analysis with the simultaneous assessment of decolorization and COD enabled clear experimental differentiation between adsorption and photocatalysis, strengthening the interpretation of TiO_2-based solar photocatalytic systems. In conclusion, solar photocatalysis using TiO_2 and the optimization of operational variables constitute an effective treatment strategy that takes advantage of solar irradiation as the primary energy source, thereby reducing dependence on conventional artificial UV irradiation. Within the scope of this study, the combination of solar radiation, continuous aeration and appropriate operating conditions demonstrated promising potential for the treatment of textile wastewater containing persistent dyes.

Academic Editor: Dmitry Yu. Murzin

Received: 30 July 2026
Revised: 16 August 2026
Accepted: 30 August 2026
Published: 14 September 2026

Keywords: solar photocatalysis; titanium dioxide (TiO_2); benzothiazole disperse dye; chemical oxygen demand; pseudo-second-order kinetics; textile effluents

1. Introduction

The pollution of aquatic ecosystems by industrial effluents continues to be one of the most important environmental challenges worldwide. Among the various industrial sectors, the textile industry is recognized as one of the largest consumers of water and chemicals and one of the main generators of highly colored wastewater. The environmental impact of these effluents extends beyond their visual appearance, as they typically contain complex mixtures of synthetic dyes, surfactants, dispersing agents, salts, and ancillary chemicals that reduce light penetration into water bodies, interfere with photosynthetic activity, and can exert toxic effects on aquatic organisms [1–4]. Over the past few decades, the continuous expansion of textile production has increased the discharge of dye-containing wastewater, highlighting the need to develop treatment technologies capable of removing persistent organic pollutants before they are released into the environment.

The synthetic dyes used in the textile dyeing and finishing processes are designed to exhibit high chemical stability under harsh environmental conditions, including resistance to radiation, oxidation, temperature variations and microbial degradation. While these characteristics are industrially desirable because they improve color durability, they also significantly hinder dye removal by conventional wastewater treatment processes [5,6]. As a result, a significant fraction of the dyes used during the dyeing process remains in the textile effluents and reaches the receiving bodies, where they can persist for long periods and contribute to environmental pollution [3,7,8].

Among the different classes of textile dyes, disperse dyes deserve special attention due to their low solubility in water and the complexity of their aromatic molecular structures. These compounds are mainly used in the dyeing of hydrophobic synthetic fibers, such as polyester and acetate, where they remain finely dispersed rather than being completely dissolved. Their chemical stability, complex aromatic structures, and limited aqueous solubility may hinder biodegradation and reduce the effectiveness of conventional treatment processes [9,10]. In addition, numerous disperse dyes contain structures based on benzothiazole, azo groups, anthraquinones, or nitroaromatic compounds, which not only determine their chromatic properties but also contribute to their environmental persistence and potential toxicity [8].

The presence of residual disperse dyes in water bodies is an environmental problem that goes beyond esthetic deterioration. The intense coloration of these effluents reduces solar radiation penetration, thereby reducing photosynthetic activity and dissolved oxygen production in aquatic ecosystems. In addition, some transformation products generated during natural degradation or incomplete treatment may exhibit toxicity equal to or even greater than that of the parent compound, representing a potential risk to aquatic organisms and, ultimately, to human health through the contamination of water resources [4,7,11,12]. These limitations have driven the development of advanced technologies capable not only of eliminating visible color but also of promoting the oxidation of persistent organic molecules into products with a lower environmental impact.

Over the last two decades, advanced oxidation processes (AOPs) have emerged as one of the most promising alternatives for the treatment of refractory organic pollutants in industrial wastewater. These technologies are based on the in situ generation of highly oxidizing species, especially hydroxyl radicals (•OH), which have a high oxidation potential and are capable of reacting with a wide variety of organic pollutants with low

selectivity [13–15]. Because of this ability, photocatalytic advanced oxidation processes have been extensively investigated for the degradation of dyes, pharmaceuticals, pesticides, and other emerging contaminants resistant to conventional biological treatments [16,17].

Among the various advanced oxidation processes, heterogeneous photocatalysis has attracted growing scientific and technological interest due to its ability to mineralize organic contaminants under relatively mild operating conditions. In this process, semiconductor materials absorb photons with energy equal to or greater than their bandgap energy, generating electron–hole pairs that initiate a series of oxidation and reduction reactions leading to the formation of reactive oxygen species capable of degrading organic molecules [4,18–20]. Heterogeneous photocatalysis can operate under relatively mild temperature and pressure conditions and may use solar radiation as an energy source; however, its practical performance depends strongly on photon utilization, reactor configuration, catalyst recovery, and water-matrix effects [13,21–23].

Among the different semiconductor materials used as photocatalysts, titanium dioxide (TiO_2) remains one of the most extensively studied due to its high photocatalytic activity, chemical stability, low toxicity, low cost and high resistance to photocorrosion [19,24]. In particular, the commercial photocatalyst Degussa P25 has become a reference material owing to its mixed anatase–rutile crystalline structure, which favors charge separation and generally provides higher photocatalytic efficiencies than many materials consisting of a single crystalline phase [18,20]. When TiO_2 is irradiated with light of sufficient energy, electrons and photogenerated holes are generated, which participate in the formation of reactive oxygen species, including hydroxyl radicals (•OH) and superoxide radicals ($O_2\bullet^-$), recognized as the main oxidizing agents responsible for the degradation of organic pollutants [25,26].

Although important advances have been made in the development of heterogeneous photocatalytic processes over recent decades, the efficiency of TiO_2-based systems depends on several operational variables that simultaneously control photon absorption, pollutant adsorption, charge separation and the generation of reactive oxygen species. Among these variables, photocatalyst concentration, solution pH, dissolved oxygen availability, irradiation intensity, and reactor configuration have been identified as factors that exert the greatest influence on the overall efficiency of the photocatalytic process [20–22]. Consequently, optimizing these operating conditions is critical to maximizing degradation efficiency while minimizing energy consumption and the amount of photocatalyst required.

The concentration of the photocatalyst directly influences the number of available photoactive sites and the probability of an interaction between contaminant molecules and the semiconductor surface. Generally, increasing the concentration of TiO_2 favors photocatalytic activity by increasing the available surface area and the number of active sites that are capable of absorbing radiation. However, above a system-specific catalyst loading, increased turbidity, light scattering, particle aggregation, and optical shielding may reduce the fraction of radiation effectively absorbed within the reactor [10,20,27]. Therefore, the optimal TiO_2 loading is system-specific and depends on reactor geometry, optical path length, pollutant concentration, irradiance, and hydrodynamic conditions [27,28].

The pH of the solution represents another operational variable of major importance because of its simultaneous influence on the photocatalyst surface and the physicochemical properties of the contaminant. In addition to modifying the chemical speciation of numerous organic compounds, solution pH affects both pollutant speciation and the surface charge of TiO_2 relative to its point of zero charge, thereby modifying adsorption, aggregation, and interfacial electron-transfer processes [10,29]. Likewise, pH variations affect the concentration of hydroxyl ions available for the formation of hydroxyl radicals (•OH) and can influence the stability of intermediate products generated during photocatalytic

oxidation. Consequently, the effect of pH should be interpreted as the result of the simultaneous interaction of several physicochemical phenomena rather than as the consequence of a single reaction mechanism [20,25].

The availability of dissolved oxygen also plays a critical role during heterogeneous photocatalysis. Oxygen acts as the main acceptor of photogenerated electrons in the TiO_2 conduction band, promoting charge separation and reducing electron–hole recombination, thereby enhancing the formation of reactive oxygen species involved in the degradation of organic pollutants [18,19]. Although the role of oxygen as an electron acceptor has been widely demonstrated for TiO_2-based photocatalytic systems, its effective contribution depends on the rate of oxygen transfer from the gas phase to the solution, a process that can become a limiting factor in insufficiently aerated systems [25,30]. Consequently, continuous aeration can increase oxygen availability and promote catalyst suspension and liquid-phase mixing; nevertheless, the magnitude of these effects depends on gas–liquid mass transfer and reactor hydrodynamics [26].

Another variable that has received increasing attention in recent years is the use of solar radiation as an energy source for photocatalytic processes. Unlike conventional systems that use ultraviolet lamps, solar radiation can considerably reduce energy consumption and operational costs, supporting the development of solar-driven environmental treatment technologies with reduced dependence on artificial UV irradiation [13,22]. However, solar photocatalysis introduces additional complexity because irradiance varies continuously depending on geographical location, the time of year, atmospheric conditions, and time of day. These fluctuations modify the incident photon flux reaching the photocatalyst and, consequently, the generation rate of electron–hole pairs. Therefore, monitoring solar irradiance during experiments is essential to ensure the reproducibility and proper interpretation of photocatalytic results.

In addition to the influence of operational variables, the mathematical description of photocatalytic degradation has become a topic of growing interest because kinetic models enable the quantitative description of system behavior and the comparison of different experimental conditions. Among the most widely used models are pseudo-first-order (PFO) and pseudo-second-order (PSO) kinetic models, which were originally developed to describe adsorption processes but were later extended to the analysis of photocatalytic systems due to their ability to mathematically represent complex processes in which adsorption, mass transfer, and surface reactions are involved simultaneously [31–33].

The pseudo-first-order kinetic model assumes that the overall rate of the process is proportional to the number of available active sites, while the pseudo-second-order model considers that the rate depends on the interaction between adsorbed molecules and the adsorbent surface [30]. Although both models were originally proposed for adsorption systems, several studies have shown that they can be used as empirical tools to describe the kinetic behavior of photocatalytic processes, providing an adequate mathematical representation of the temporal evolution of pollutant degradation [34,35]. However, it is important to note that a better statistical fit does not necessarily constitute evidence of the molecular mechanism responsible for the photocatalytic reaction; rather, it indicates that a given model reproduces the experimental data more accurately [35].

Various studies have reported the photocatalytic degradation of textile dyes using TiO_2 under ultraviolet or solar irradiation. However, most of these studies have focused on optimizing a single operational variable or solely on evaluating decolorization efficiency, without simultaneously considering the reduction in chemical oxygen demand (COD), the influence of continuous aeration, and the kinetic behavior of the process under natural solar irradiation conditions [26,36,37]. In addition, limited information is available on the solar photocatalytic degradation of benzothiazole-based disperse dyes using an experimental

approach that integrates TiO_2 concentration, pH, aeration and kinetic analysis within a single experimental system.

Although decolorization is one of the most widely used indicators for assessing the efficiency of photocatalytic processes, the disappearance of visible color does not necessarily imply complete degradation or mineralization of the contaminant. The breakdown of the chromophore groups responsible for radiation absorption in the visible region usually occurs during the early stages of photocatalytic oxidation, while the transformation of intermediates into lower-molecular-weight compounds and, eventually, carbon dioxide, water, and inorganic ions requires longer irradiation times and the sustained generation of reactive oxygen species [20,25]. Consequently, the disappearance of color alone does not provide sufficient evidence of the environmental efficiency of the treatment.

For this reason, the simultaneous determination of chemical oxygen demand (COD) has become increasingly important in the evaluation of photocatalytic processes. Unlike UV–Visible absorbance measurements, which primarily reflect changes in chromophoric structures, COD quantifies the amount of oxidizable organic matter present in the solution and provides complementary information on the degree of oxidation achieved during treatment. The joint evaluation of decolorization and COD helps distinguish the initial disruption of chromophoric structures from the progressive oxidation of the remaining organic matter. A decrease in COD supports partial or progressive mineralization, although it does not demonstrate complete conversion to CO_2, H_2O, and inorganic ions [10,21,38,39].

Another relevant aspect is the chemical nature of the dye investigated. The compound 2-(4-amino-2-nitrophenyl)-1,3-benzothiazole belongs to the family of benzothiazole-derived disperse dyes, characterized by heterocyclic aromatic structures with high chemical stability and significant resistance to conventional degradation processes [8,40]. In recent years, the oxidation of benzothiazole derivatives has attracted increasing interest because their transformation pathways generally involve multiple intermediate products before reaching high degrees of oxidation, highlighting the need to complement the evaluation of decolorization with indicators of the mineralization or oxidation of organic matter [41].

From an environmental engineering perspective, the implementation of photocatalytic processes on a larger scale requires consideration of not only the intrinsic properties of the photocatalyst but also variables related to reactor design, spatial radiation distribution, oxygen transfer, particle suspension, and system hydrodynamics. These factors simultaneously affect photon utilization, mass transfer, catalyst suspension, and the overall treatment rate. Consequently, results obtained under natural solar irradiation provide useful information for subsequent reactor design, although laboratory observations must be validated through optical, hydrodynamic, energetic, and pilot-scale studies before industrial extrapolation [20,38,42].

Although considerable research has been conducted on the photocatalytic degradation of textile dyes, most studies have focused on azo or reactive dyes and have used artificial ultraviolet radiation. In contrast, comprehensive information on the solar photocatalytic degradation of benzothiazole-derived disperse dyes remains limited, particularly regarding the simultaneous evaluation of photocatalyst concentration, solution pH, and continuous aeration, together with chemical oxygen demand reduction and kinetic model comparisons under natural solar irradiation conditions [26,36,37]. This knowledge gap makes it difficult to establish clear relationships between operational variables and the overall efficiency of the photocatalytic process, as well as to define design criteria applicable to environmental treatment systems.

In this context, the present study aimed to evaluate the influence of TiO_2 concentration, solution pH and continuous aeration on the solar photocatalytic degradation of the disperse dye 2-(4-amino-2-nitrophenyl)-1,3-benzothiazole using commercial TiO_2 (Degussa

P25) under natural solar irradiation conditions. The efficiency of the process was evaluated in terms of dye decolorization and chemical oxygen demand reduction, while the kinetic behavior was analyzed using pseudo-first-order and pseudo-second-order models to identify which model best described the experimental evolution of the process within the range of operational conditions investigated. The results contribute to the understanding of solar photocatalysis applied to persistent disperse dyes and provide laboratory-scale information for optimizing the evaluated operating variables. Further validation using real textile wastewater and pilot-scale reactors is required before the scalability of the process can be established.

2. Materials and Methods

2.1. Equipment, Materials and Reagents

The photocatalytic degradation tests of the dispersed textile dye were carried out using the equipment, materials and reagents presented in Table 1.

Table 1. List of equipment, materials and reagents.

Items	Specifications
Equipment	
UV–Visible Spectrophotometer	Model UV1600PC, Brand: W&J Instrument Co., Ltd., Changzhou, China
Analytical Balance	Model Adventurer AX224, Brand: OHAUS, Parsippany, NJ, USA
Pyranometer	Class 1, Model: SR15, Brand: Hukseflux, Delft, The Netherlands
Centrifuge	Model: BKC-TH20RL, Brand: BIOBASE, Jinan, China
Air Pump	4 L/min, Model WP 3550, Brand: Sobo, Zhongshan, China
Materials	
Rotating Sample Container	Glass base and walls
Borosilicate glass containers	Solution preparation
Reagents	
Disperse Textile Dye	2-(4-amino-2-nitrophenyl)-1,3-benzothiazole, supplied by SOQUITEX ING SR, Lima, Peru
Titanium Dioxide (TiO_2)	P25, Brand: Degussa, Essen, Germany
Sulfuric Acid (H_2SO_4)	Diluted solution for pH adjustment, Brand: Merck, Darmstadt, Germany
Sodium Hydroxide (NaOH)	Diluted solution for pH adjustment, Brand: Merck, Darmstadt, Germany

The main photocatalyst used in this research was commercial titanium dioxide P25 (Degussa), selected for its high photocatalytic activity and widespread use as a reference material in studies on the degradation of organic pollutants. The material was supplied as a white powder consisting of a crystalline mixture of approximately 80% anatase and 20% rutile, with an average particle size of 21 $\pm$ 5 nm, a specific surface area (BET) of 50 m^2/g, a specific pore volume of 0.30 cm^3/g, and a purity greater than 99.5% TiO_2. The reported physicochemical properties were obtained from the technical specifications provided by the manufacturer.

The dye used in the experiments was 2-(4-amino-2-nitrophenyl)-1,3-benzothiazole, a representative disperse dye used in the dyeing of synthetic fibers. Dilute solutions of

sulfuric acid and analytical-grade sodium hydroxide (Merck) were used to adjust the pH of the experimental solutions. All reagents were used without further purification.

2.2. Determination of the Point of Zero Charge (PZC)

In order to interpret the effect of pH on the electrostatic interactions between the photocatalyst surface and the dye molecules, the point of zero charge (PZC) of titanium dioxide P25 was experimentally determined. This parameter represents the pH value at which the TiO_2 surface has a net charge equal to zero, and it constitutes a fundamental criterion for analyzing the phenomena of electrostatic adsorption and repulsion during heterogeneous photocatalysis.

The PZC of TiO_2 was determined using the pH drift method. Briefly, a series of 0.01 M NaCl solutions were prepared using NaCl as the background electrolyte, and their initial pH (pH_0) was adjusted from 2 to 12 by adding 0.1 M HCl or 0.1 M NaOH solutions. Subsequently, a known amount of TiO_2 was added to each solution and the suspensions were maintained under constant stirring for 24 h at room temperature until equilibrium was reached. Finally, the equilibrium pH (pHf) was determined and a plot of ΔpH ($pHf - pH_0$) versus pH_0 was constructed. The PZC was determined as the pH at which $\Delta pH = 0$, corresponding to the condition where the TiO_2 surface has zero net charge. Under the experimental conditions of this study, the PZC was determined to be pHpzc = 6.2.

2.3. Preparation of the Coloring Solution

Due to the hydrophobic nature of the disperse dye 2-(4-amino-2-nitrophenyl)-1,3-benzothiazole, its solubility in water is limited; therefore, the dye does not form a true solution but rather a stable colloidal dispersion. For this reason, the preparation procedure was designed to maximize the apparent dispersion of the dye prior to photocatalytic treatment. To prepare the stock dispersion, distilled water was preheated to 80 °C and subjected to vigorous stirring. Subsequently, the dye was gradually added under continuous stirring until a homogeneous dispersion was obtained. The initial dye concentration was 200 mg/L [2].

Heating was used only during the preparation stage to enhance dye dispersion. Once a homogeneous dispersion was obtained, it was allowed to cool naturally to room temperature before the photocatalytic experiments were initiated. All experiments were subsequently carried out under natural environmental conditions, at temperatures ranging from approximately 22 to 28 °C, without thermostatic control. Due to the low solubility of the dye, the system remained in dynamic equilibrium between the dissolved fraction and finely dispersed particles. As the dissolved fraction was consumed during photocatalysis, this equilibrium promoted the progressive transfer of dye molecules from the dispersed phase to the dissolved phase, maintaining dye availability for the degradation process.

2.4. Preparation of Treatment Solutions

Photocatalytic experiments were performed using the dye stock dispersion prepared according to the procedure described in the previous section. The treatment mixtures had a total volume of 1200 mL, with pH systematically varied at five levels (5, 6, 7, 8 and 9) and TiO_2 P25 concentration at two levels (200 and 400 ppm), to evaluate the combined effect of both variables on dye decolorization and photocatalytic degradation.

As a control, an additional set of samples without TiO_2 was prepared to evaluate the possible contribution of direct photolysis under solar irradiation. For each TiO_2 treatment, experiments were conducted with and without forced aeration, allowing the effects of aeration on the photocatalytic process to be evaluated.

The initial dye concentration was kept constant in all experiments, and the combinations of pH, TiO_2 concentration, and aeration conditions were established according to the experimental design summarized in Table 2.

Table 2. Flowchart for preparing treatment solutions.

TiO_2 Concentration	pH									
	5		6		7		8		9	
	Aeration		Aeration		Aeration		Aeration		Aeration	
	Yes	No	Yes	No	Yes	No	Yes	No	Yes	No
200 ppm	✓	✓	✓	✓	✓	✓	✓	✓	✓	✓
400 ppm	✓	✓	✓	✓	✓	✓	✓	✓	✓	✓
absence of TiO_2	✓	—	✓	—	✓	—	✓	—	✓	—

Note: ✓, experiment conducted; —, experiment not conducted.

The experimental conditions evaluated included two TiO_2 concentrations (200 and 400 ppm), five pH values, and two aeration conditions (with and without aeration). Control experiments without TiO_2 were also conducted under the corresponding aerated and non-aerated conditions to assess the contribution of direct photolysis under the same solar irradiation conditions. This experimental strategy enabled the systematic evaluation of the influence of the main operating variables on the efficiency of the photocatalytic process and its capacity to remove the organic contaminant from the reaction medium [27,37,43].

2.5. Photocatalytic Reactor and Experimental Procedure

Once the treatment mixtures were prepared, the samples were subjected to solar irradiation using a photocatalytic reactor designed to enhance the utilization of incident solar radiation and reduce experimental variability associated with vessel position relative to the apparent motion of the sun. The photocatalytic process was conducted by irradiating TiO_2 with solar radiation, thereby promoting the generation of reactive oxygen species involved in dye degradation, according to the mechanism described for heterogeneous photocatalytic systems [19,27,37].

The experimental system consisted of a rotating platform on which the reaction vessels were placed. The base and inner walls of the reactor were covered with mirrors to reflect solar radiation toward the reaction vessels and enhance light exposure. Additionally, the continuous rotation of the platform provided more uniform exposure for the vessels, minimizing differences associated with orientation and shading during the experimental period [38].

Figure 1 shows the experimental system used during the photocatalytic experiments, including the arrangement of the vessels on the rotating platform and the reflective mirrors located at the base and along the inner walls of the reactor.

Solar irradiance was continuously monitored using a calibrated pyranometer throughout the experimental period. The experiments were carried out under natural environmental conditions during January, with a mean solar irradiance of 492 ± 58 W/m^2 recorded over the experimental period. The ambient temperature ranged from approximately 22 to 28 °C [44]. Samples were collected periodically between 06:00 and 18:00 h. After each sampling, the suspensions were centrifuged at 10,000 rpm and subsequently filtered prior to spectrophotometric analysis. Chemical oxygen demand (COD) was determined in the initial and final samples for each treatment.

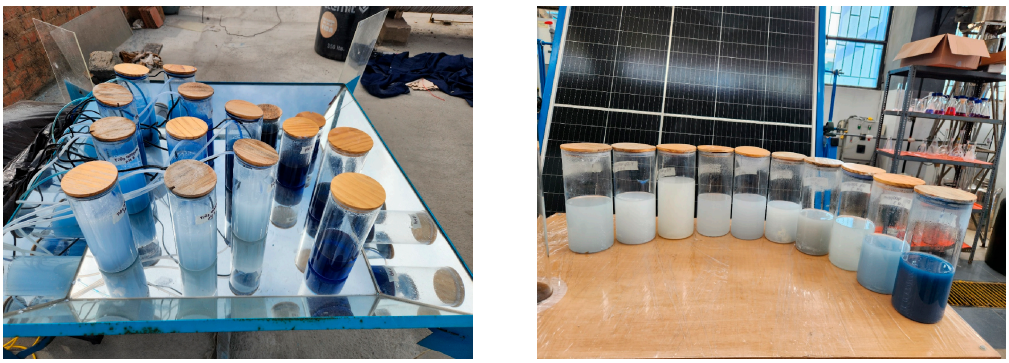

(**a**) (**b**)

Figure 1. Solar photocatalytic treatment of the textile dye under natural solar radiation: (**a**) samples during solar exposure; (**b**) samples after completion of the photocatalytic treatment.

Each experimental condition was evaluated in duplicate (n = 2). The reported dye concentration and COD values represent the means of duplicate measurements, and the associated variability is reported as the standard deviation (± SD).

2.6. Analytical Methods

2.6.1. Determination of Dye Concentration

The residual dye concentration was determined by UV–Visible spectrophotometry using a spectrophotometer (see Table 1 for model specifications). Prior to analysis, the samples were centrifuged at 10,000 rpm for the time specified in the experimental procedure to separate suspended TiO_2 particles. When necessary, the samples were also filtered to minimize interference from light scattering caused by residual photocatalyst particles. The residual dye concentration was calculated using a previously established calibration curve based on absorbance measurements at the dye's maximum absorption wavelength (λmax).

2.6.2. Determination of Chemical Oxygen Demand (COD)

The oxidation of organic matter during dye degradation was assessed by measuring chemical oxygen demand (COD) using the potassium dichromate method in a strongly acidic medium, following standard procedures for wastewater analysis. Due to the high initial dye concentration, the sample corresponding to time zero was diluted at a ratio of 1:20 before digestion to maintain the measurement within the working range of the analytical method. For samples collected during photocatalytic treatment, the dilution factor was adjusted according to the progressive decrease in the organic load.

The samples were digested using a COD digester under the conditions recommended by the reagent manufacturer. Subsequently, absorbance was measured using a calibrated spectrophotometer. The values obtained were expressed as mg O_2/L and were used as an indicator of organic matter oxidation during the photocatalytic process. The decrease in COD was used as a complementary indicator to decolorization for assessing the degree of organic matter oxidation, helping to distinguish color removal from the progressive oxidation of the organic matter remaining in the reaction medium.

2.7. Kinetic Analysis and Data Processing

2.7.1. Calculation of the Adsorbed Quantity

The experimental concentrations obtained during the photocatalytic treatment were used to calculate the apparent amount of dye removed per unit mass of TiO_2, using

Equation (1), which relates the volume of the solution, the initial concentration of the dye, the concentration at any time and the mass of the photocatalyst q_t.

$$q_t = \frac{V(C_0 - C_t)}{W} \quad (1)$$

where

V: Solution volume (L);
W: Adsorbent mass (g);
C_0: Initial dye concentration (mg/L);
C_t: Dye concentration over time (mg/L) t;
q_t: Apparent amount of dye removed per unit mass of TiO_2 (mg/g).

In the present study, the variable represents an apparent kinetic variable calculated from the decrease in the concentration of the dye in solution and was used only for the adjustment of the kinetic models q_t .

2.7.2. Kinetic Models

To describe the kinetic behavior of the photocatalytic process, the experimental data were fitted using the Lagergren pseudo-first-order (PFO) and Ho–McKay pseudo-second-order (PSO) kinetic models, as both models have been widely used to describe heterogeneous adsorption processes and as empirical models in photocatalytic systems [30,45]. In addition to the PFO and PSO models, the Elovich kinetic model and the Weber–Morris intraparticle-diffusion model were evaluated to provide complementary descriptions of the time-dependent apparent dye removal [46,47]. The corresponding fitted parameters and goodness-of-fit statistics are provided in Appendix A.

Classical equilibrium adsorption isotherms, including the Langmuir, Freundlich, Temkin, Dubinin–Radushkevich, and Sips models, were not fitted to the experimental data because this study was not designed as an equilibrium adsorption investigation. Specifically, the experiments were conducted at a single initial dye concentration, and q_t represents an apparent kinetic quantity derived from the decrease in dye concentration during the simultaneous occurrences of adsorption and photocatalytic degradation. Therefore, the available data did not provide independent equilibrium $C_e - q_e$ data pairs, where C_e is the equilibrium dye concentration in solution, required for a rigorous adsorption isotherm analysis.

The pseudo-first-order model is as follows:

$$\frac{dq_t}{dt} = k_1(q_e - q_t) \quad (2)$$

By integrating Equation (2), we obtain the following:

$$\ln(q_e - q_t) = \ln q_e - k_1 t \quad (3)$$

The pseudo-second-order model is as follows:

$$\frac{dq_t}{dt} = k_2(q_e - q_t)^2 \quad (4)$$

By integrating Equation (4), we obtain the following:

$$\frac{t}{q_t} = \frac{1}{k_2 {q_e}^2} + \frac{t}{q_e} \quad (5)$$

Equations (3) and (5) were used to perform a linear fit of the experimental data and to obtain the corresponding kinetic parameters.

2.7.3. Statistical Treatment

The kinetic parameters obtained from the pseudo-first-order (PFO) and pseudo-second-order (PSO) models are presented in Tables 3–10, in numerical order. Tables 3 and 4 correspond to the PFO and PSO models, respectively, for the first experimental condition; Tables 5–10 present the corresponding results for the remaining experimental conditions. For the PFO model, the linear regression parameters are defined as $m = -k_1$ and $b = lnq_e$ whereas for the PSO model, they are defined as $m = 1/q_e$ and $b = 1/(k_2 q_e^2)$.

The coefficient of determination (R^2) and chi-square statistic (χ^2) were used to compare the empirical descriptive performance of the kinetic models. Higher R^2 and lower χ^2 values indicate better agreement between experimental and model-calculated values.

3. Results

This section presents the experimental results obtained during the photocatalytic degradation of the disperse dye 2-(4-amino-2-nitrophenyl)-1,3-benzothiazole under different operating conditions. The results are organized according to the experimental variables evaluated, including photocatalyst concentration, solution pH, and aeration conditions. For ease of interpretation, the complete experimental data are presented in Appendix A Tables A1–A4, and the figures show the temporal evolution of dye concentration and comparisons among different operating conditions. Subsequently, the experimental data were fitted using pseudo-first-order (PFO) and pseudo-second-order (PSO) kinetic models, with the corresponding parameters presented in the respective tables.

3.1. Effect of pH on Dye Discoloration Using 200 ppm TiO_2 with Aeration

The experiments were performed using a constant TiO_2 P25 concentration of 200 ppm, continuous aeration at 4 L/min and five pH values (5, 6, 7, 8 and 9). The complete experimental data obtained during photocatalytic treatment are presented in Appendix A Table A1, including time-dependent dye concentrations and final chemical oxygen demand (COD) values.

The temporal evolution of the dye concentration, constructed from the experimental data in Table A1, is presented in Figure 2.

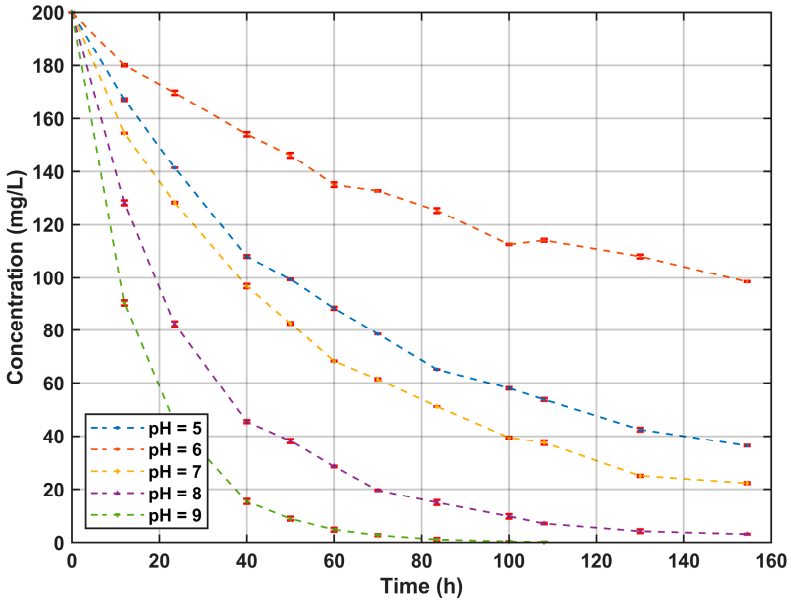

Figure 2. Temporal evolution of the dye concentration for different pH values using 200 ppm of TiO_2 with aeration. Data are presented as the mean ± standard deviation of duplicate measurements (n = 2).

Figure 2 shows a progressive decrease in dye concentration during photocatalytic treatment for all pH conditions evaluated. However, the experimental curves show differences in the rate of decrease in concentration and in the residual values reached at the end of the treatment. In order to quantitatively describe the observed kinetic behavior, the experimental data were initially adjusted using the pseudo-first-order model. Table 3 presents the kinetic parameters obtained by linear fitting of the pseudo-first-order model for the different pH conditions evaluated.

Table 3. Kinetic parameters obtained using the pseudo-first-order model for 200 ppm of TiO_2 with aeration.

Parameters	pH				
	5	**6**	**7**	**8**	**9**
m	0.0231	0.0183	0.0275	0.0370	0.0667
b	6.8396	6.3074	6.9957	6.9505	6.9995
k_1 (h^{-1})	0.0231	0.0183	0.0275	0.0370	0.0667
q_e (mg/g)	934.16	548.64	1091.96	1043.75	1096.09
R^2	0.9709	0.9823	0.9311	0.9848	0.9949
χ^2	228.31	61.53	536.46	37.39	78.29

m = slope of the linear regression; b = intercept of the linear regression.

Subsequently, the same experimental data were adjusted using the pseudo-second-order model. Table 4 summarizes the parameters obtained using the pseudo-second-order model for the same experimental conditions.

Table 4. Kinetic parameters obtained using the pseudo-second-order model for 200 ppm of TiO_2 with aeration.

Parameters	pH				
	5	**6**	**7**	**8**	**9**
m	0.0007	0.0012	0.0008	0.0008	0.0009
b	0.0599	0.1181	0.0447	0.0197	0.0084
k_2 ($mg^{-1}g\,h^{-1}$)	1.06×10^{-5}	1.28×10^{-5}	1.44×10^{-5}	3.68×10^{-5}	9.75×10^{-5}
q_e (mg/g)	1251.31	810.41	1243.12	1172.21	1101.59
R^2	0.9936	0.9723	0.9984	0.9972	0.9974
χ^2	3.1459	4.2203	1.7230	7.8310	11.5117

m = slope of the linear regression; b = intercept of the linear regression.

In order to illustrate the quality of the fit obtained by the pseudo-second-order model, Figure 3 presents a comparison between the experimental values and the values calculated for the selected extreme conditions (pH 6 and pH 9).

The curves show an adequate agreement between the experimental data and the values calculated for both pH conditions. The quantitative comparison between the kinetic models is presented later, based on the statistical parameters obtained for all experimental conditions.

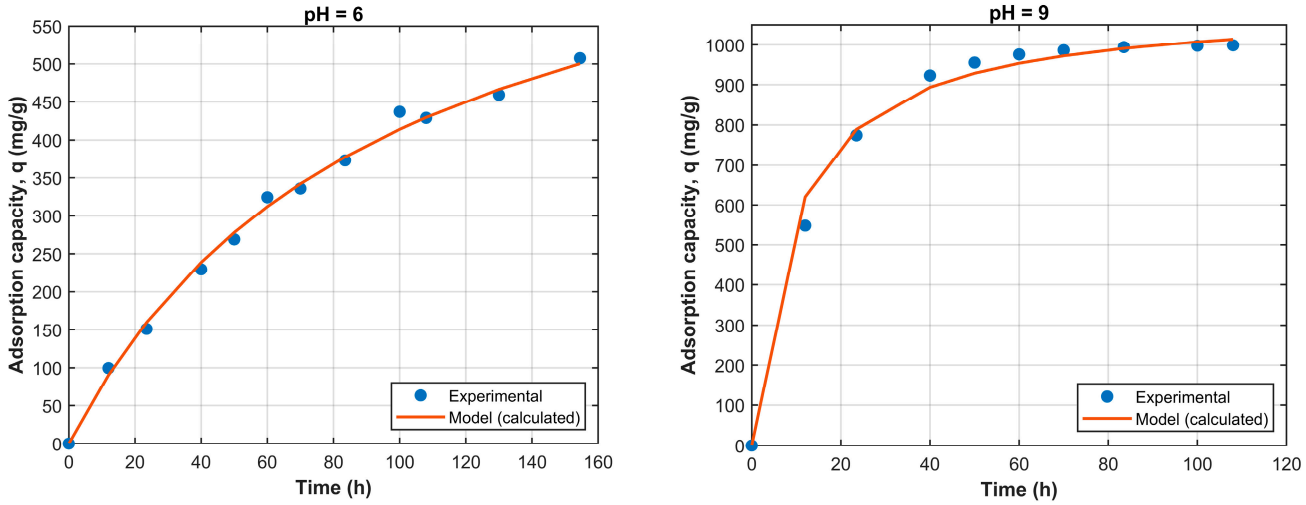

Figure 3. Comparison of experimental and calculated values using the pseudo-second-order model for 200 ppm TiO_2; with aeration: (**a**) pH 6; (**b**) pH 9.

3.2. Effect of pH on Dye Discoloration Using 200 ppm TiO_2 Without Aeration

The results for tests performed with 200 ppm TiO_2 in the absence of aeration are presented in Table A2 of Appendix A. The temporal evolution of the dye concentration for the different pH values is shown in Figure 4 (See Table A2 in Appendix A).

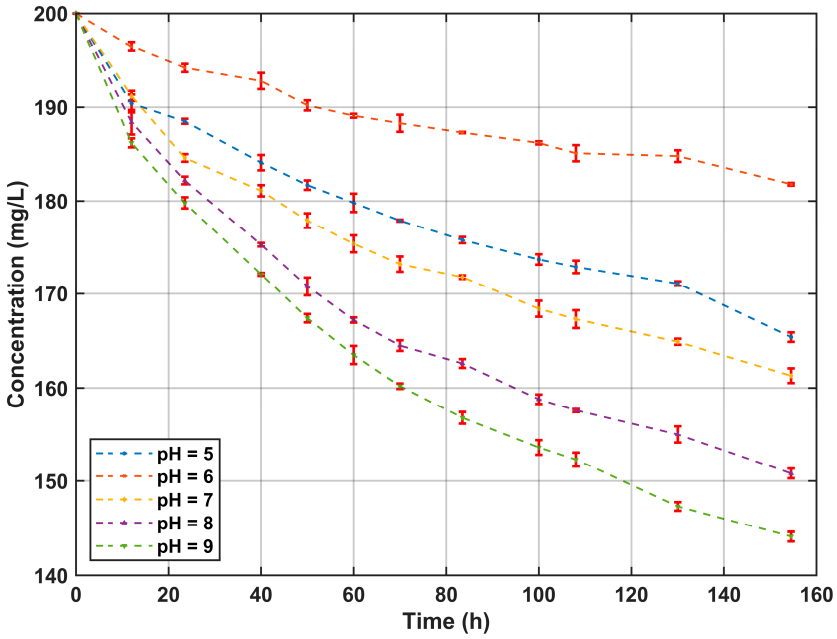

Figure 4. Temporal evolution of the dye concentration for different pH values using 200 ppm of TiO_2 without aeration. Data are presented as the mean ± standard deviation of duplicate measurements (n = 2).

The kinetic parameters obtained by the pseudo-first-order and pseudo-second-order models are presented in Tables 5 and 6, respectively.

Table 5. First-order pseudo-model without aeration and 200 ppm of TiO_2.

Parameters	pH				
	5	**6**	**7**	**8**	**9**
m	0.0134	0.0143	0.0172	0.0183	0.0197
b	5.0716	4.4886	5.2588	5.5091	5.6977
k_1 (h^{-1})	0.0134	0.0143	0.0172	0.0183	0.0197
q_e (mg/g)	159.43	89.00	192.26	246.93	298.19
R^2	0.9954	0.9889	0.9899	0.9964	0.9693
χ^2	53.440	4.172	6.081	3.076	20.992

m = slope of the linear regression; b = intercept of the linear regression.

Table 6. Second-order pseudo-model without aeration and 200 ppm of TiO_2.

Parameters	pH				
	5	**6**	**7**	**8**	**9**
m	0.0050	0.0080	0.0040	0.0030	0.0026
b	0.2702	0.6433	0.2403	0.1879	0.1676
k_2 ($mg^{-1}g\,h^{-1}$)	9.22×10^{-5}	9.94×10^{-5}	6.55×10^{-5}	4.81×10^{-5}	4.06×10^{-5}
q_e (mg/g)	200.24	125.00	251.93	332.28	382.91
R^2	0.9698	0.9648	0.9871	0.9942	0.9871
χ^2	8.9564	1.9757	2.3728	1.1981	1.8462

m = slope of the linear regression; b = intercept of the linear regression.

The comparison between the experimental values and those calculated using the pseudo-second-order model for pH 6 and pH 9 is presented in Figure 5.

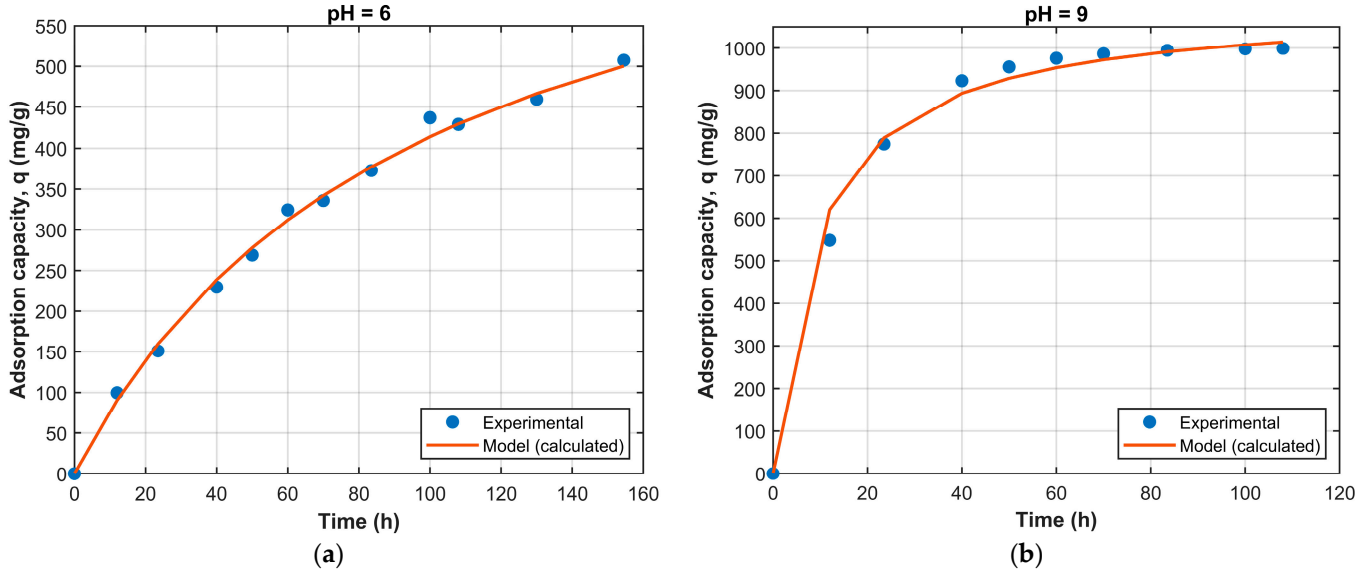

Figure 5. Comparison of experimental and calculated values using the pseudo-second-order model for 200 ppm TiO_2; without aeration: (**a**) pH 6; (**b**) pH 9.

3.3. Effect of pH on Dye Discoloration Using 400 ppm TiO_2 with Aeration

Tests performed with a concentration of 400 ppm TiO_2 P25 and an aeration flow rate of 4 L/min were evaluated for pH values of 5, 6, 7, 8 and 9. The complete experimental data

on dye concentration as a function of time are presented in Table A3 of Appendix A. The last row of this table contains the final values of chemical oxygen demand (COD) obtained for each pH condition. The temporal evolution of the dye concentration, obtained from the data in Table A3 (See Appendix A), is presented in Figure 6.

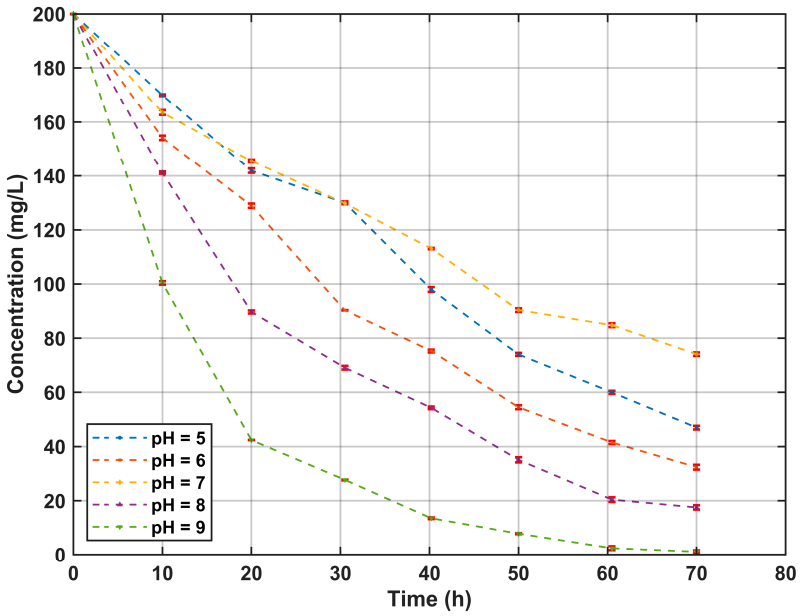

Figure 6. Time evolution of dye concentration for different pH values using 400 ppm TiO_2 with aeration. Data are presented as the mean ± standard deviation of duplicate measurements (n = 2).

Figure 6 shows a progressive decrease in the concentration of the dye during the irradiation period for all pH values evaluated. The curves show differences in the rates of decrease and in the residual concentrations reached at the end of treatment.

The experimental data in Table A3 were initially adjusted using the pseudo-first-order model. The kinetic and statistical parameters obtained are presented in Table 7.

Table 7. Kinetic parameters obtained using the pseudo-first-order model for 400 ppm of TiO_2 with aeration.

Parameters	pH				
	5	**6**	**7**	**8**	**9**
m	0.0392	0.0460	0.0405	0.0604	0.0770
b	6.8794	6.9435	6.6076	7.1155	7.0152
k_1 (h^{-1})	0.0392	0.0460	0.0405	0.0604	0.0770
q_e (mg/g)	971.99	1036.39	740.73	1230.87	1113.48
R^2	0.9251	0.9544	0.9469	0.8946	0.9721
χ^2	551.92	421.34	200.07	768.39	101.37

m = slope of the linear regression; b = intercept of the linear regression.

Subsequently, the same experimental data were adjusted using the pseudo-second-order model, whose parameters are presented in Table 8.

Table 8. Kinetic parameters obtained using the pseudo-second-order model for 400 ppm of TiO_2 with aeration.

Parameters	pH				
	5	6	7	8	9
m	0.0004	0.0006	0.0008	0.0007	0.0009
b	0.0652	0.0393	0.0539	0.0246	0.0097
k_2 ($mg^{-1}g\,h^{-1}$)	2.03×10^{-6}	9.64×10^{-6}	1.32×10^{-5}	2.16×10^{-5}	7.51×10^{-5}
q_e (mg/g)	2746.29	1623.77	1183.44	1372.93	1172.56
R^2	0.7086	0.9689	0.9237	0.9882	0.9965
χ^2	8.8156	4.5240	8.9156	5.4631	7.5530

m = slope of the linear regression; b = intercept of the linear regression.

In order to graphically show the fit of the pseudo-second-order model, Figure 7 presents a comparison between the experimental values and the calculated values for pH 6 and pH 9, which were selected as representative conditions of the observed extreme behaviors.

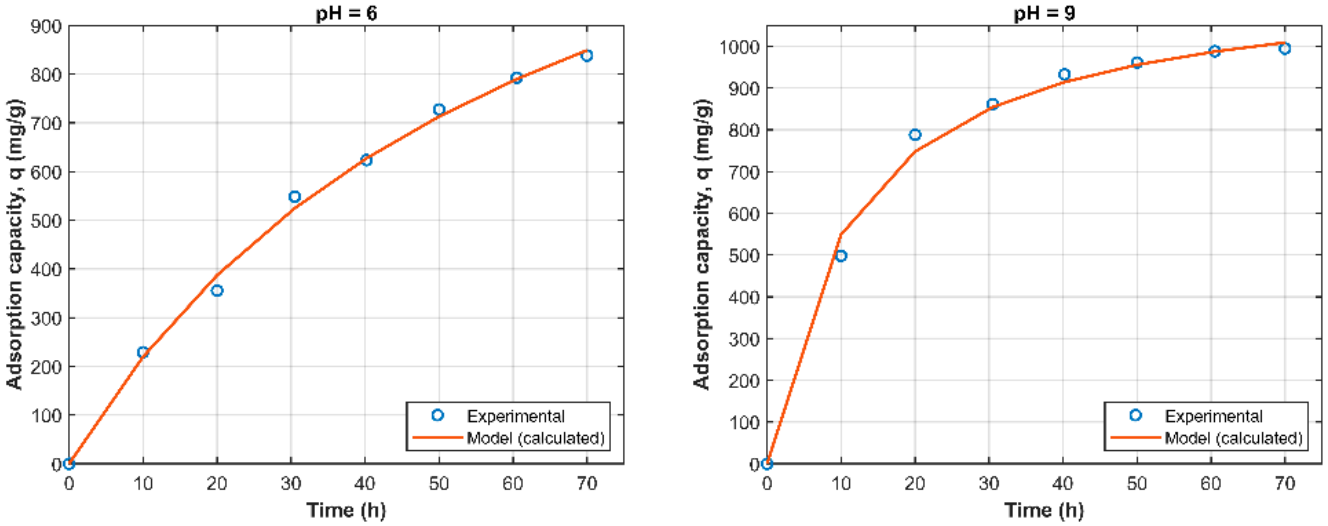

Figure 7. Comparison of experimental and calculated values using the pseudo-second-order model for 400 ppm TiO_2; with aeration: (**a**) pH 6; (**b**) pH 9.

3.4. Effect of pH on Dye Discoloration Using 400 ppm TiO_2 Without Aeration

The results obtained with 400 ppm TiO_2 in the absence of aeration are presented in full in Table A4 of Appendix A. This table contains the dye concentrations recorded during treatment for the different pH values, as well as the final COD values included in its last row. The temporal evolution of the dye concentration, constructed from the data in Table A4 (see Appendix A), is presented in Figure 8.

Figure 8 shows a progressive decrease in dye concentration during treatment for all pH values. The residual concentrations obtained in the absence of aeration were different from those recorded under aeration, although the interpretation of these differences is presented later in the Discussion. The experimental data in Table A4 were adjusted using the pseudo-first-order model. The corresponding parameters are presented in Table 9.

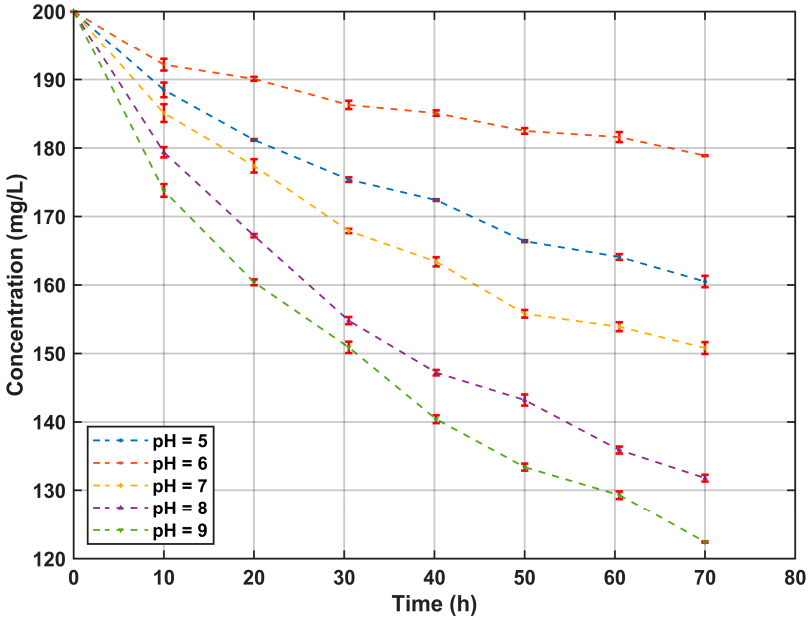

Figure 8. Temporal evolution of the dye concentration for different pH values using 400 ppm of TiO_2 without aeration. Data are presented as the mean ± standard deviation of duplicate measurements (n = 2).

Table 9. Kinetic parameters obtained by the pseudo-first-order model for 400 ppm TiO_2 without aeration.

Parameters	pH				
	5	6	7	8	9
m	0.0043	0.0018	0.0075	0.0069	0.0070
b	6.6124	6.7119	6.4084	6.7749	6.8505
k_1 (h^{-1})	0.0043	0.0018	0.0075	0.0069	0.0070
q_e (mg/g)	744.30	822.13	606.89	875.62	944.33
R^2	0.9659	0.9217	0.9750	0.9671	0.9581
χ^2	58.51	79.27	49.14	95.03	166.48

m = slope of the linear regression; b = intercept of the linear regression.

The same data were subsequently adjusted using the pseudo-second-order model, whose kinetic and statistical parameters are presented in Table 10.

Table 10. Kinetic parameters obtained using the pseudo-second-order model for 400 ppm of TiO_2 without aeration.

Parameters	pH				
	5	6	7	8	9
m	0.0030	0.0066	0.0023	0.0018	0.0017
b	0.1532	0.2396	0.1192	0.0823	0.0654
k_2 ($mg^{-1}g\,h^{-1}$)	5.86×10^{-5}	1.83×10^{-4}	4.62×10^{-5}	3.85×10^{-5}	4.45×10^{-5}
q_e (mg/g)	333.76	151.10	426.10	561.97	585.73
R^2	0.9799	0.9499	0.9788	0.9936	0.9864
χ^2	0.8933	2.2891	1.3259	0.5920	1.9222

m = slope of the linear regression; b = intercept of the linear regression.

Figure 9 presents a comparison between the experimental values and those calculated using the pseudo-second-order model for pH 6 and pH 9.

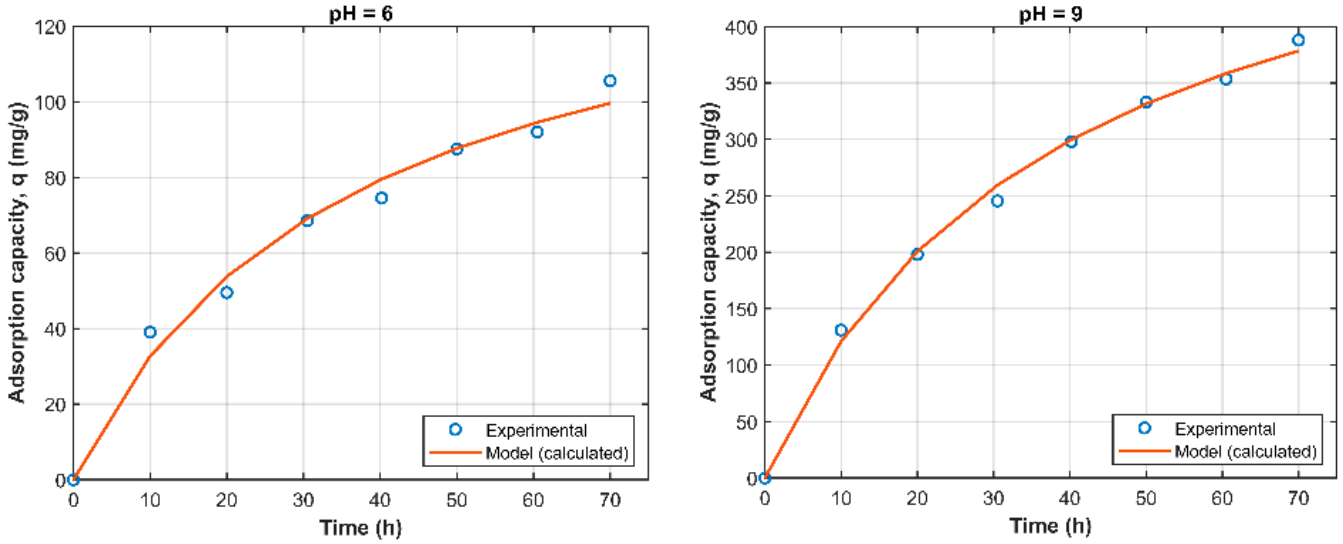

(**a**) (**b**)

Figure 9. Comparison of experimental and calculated values using the pseudo-second-order model for 400 ppm TiO_2; without aeration: (**a**) pH 6; (**b**) pH 9.

3.5. Influence of Aeration

The influence of aeration was evaluated by directly comparing the apparent quantity profiles obtained with and without air supply. For 200 ppm TiO_2, comparisons for pH 6 and pH 9 are presented in Figures 10 and 11, respectively.

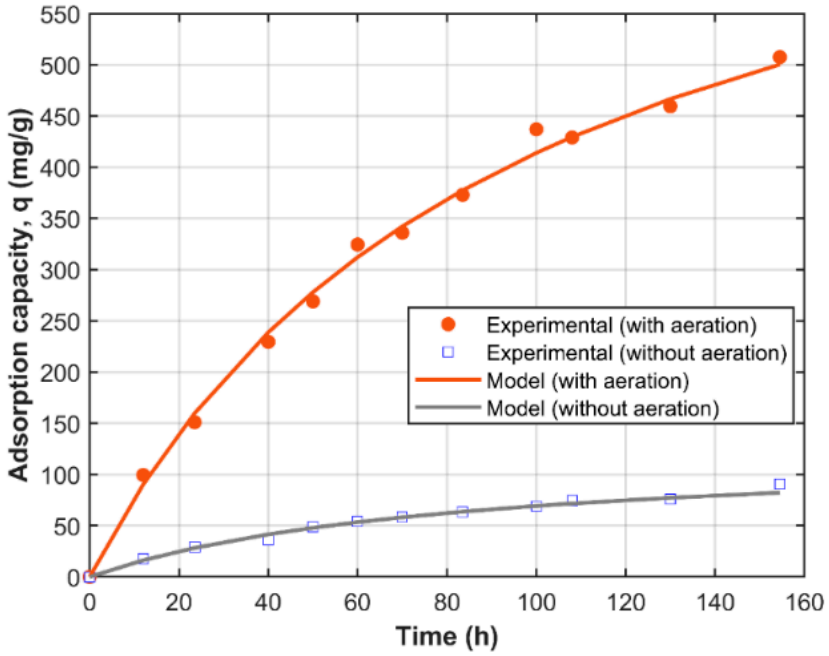

Figure 10. Comparison of the apparent amount removed with and without aeration using 200 ppm TiO_2 at pH 6.

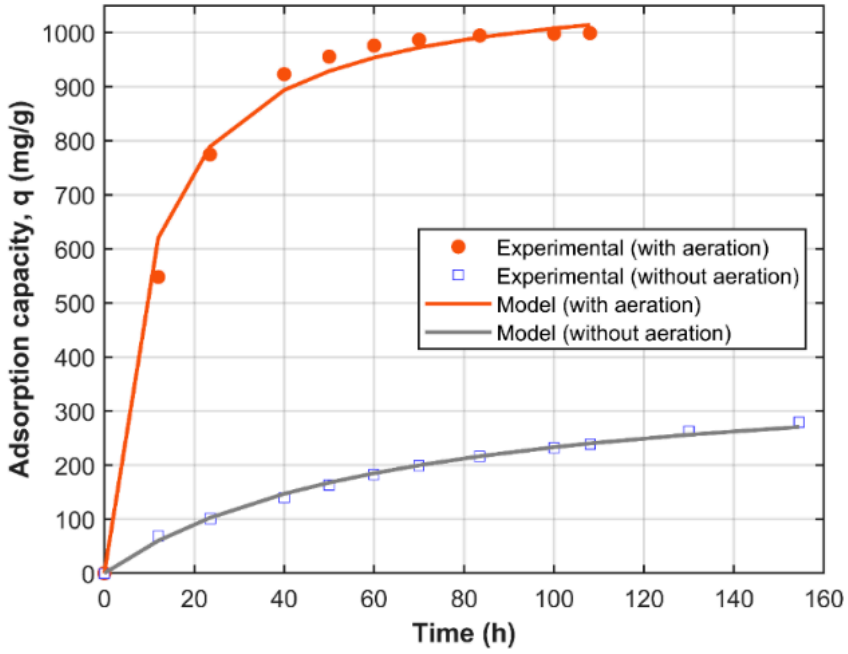

Figure 11. Comparison of the apparent amount removed with and without aeration using 200 ppm TiO_2 at pH 9.

For 400 ppm TiO_2, comparisons at pH 6 and pH 9 are presented in Figures 12 and 13, respectively.

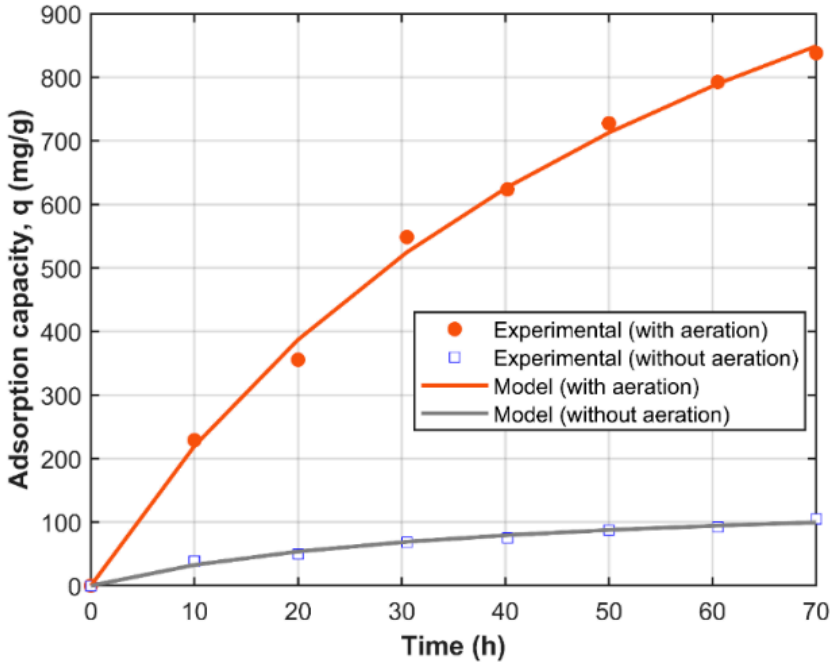

Figure 12. Comparison of the apparent amount removed with and without aeration using 400 ppm TiO_2 at pH 6.

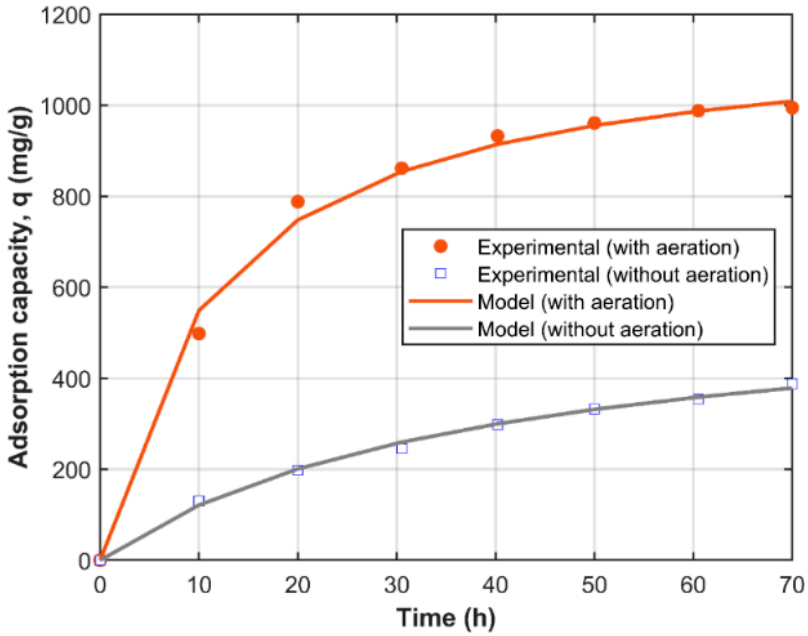

Figure 13. Comparison of the apparent amount removed with and without aeration using 400 ppm TiO_2 at pH 9.

3.6. Final Values of Chemical Oxygen Demand

The initial sample of the dye presented a COD of 423.7 ± 6.2 mg/L. The final COD values obtained after treatment are found in the last row of Appendix A Tables A1–A4. Table A1 corresponds to treatment with 200 ppm of TiO_2 and aeration; Table A2, at 200 ppm without aeration; Table A3, at 400 ppm with aeration; and Table A4, at 400 ppm without aeration. These values allow for an objective comparison of the residual organic load obtained under the different combinations of pH, TiO_2 concentration, and aeration conditions.

The interpretation of COD decrease in terms of dye oxidation, intermediate formation, and partial mineralization is developed in Section 4.

4. Discussion

4.1. Influence of TiO_2 Concentration

Increasing the TiO_2 concentration from 200 to 400 ppm enhanced the photocatalytic degradation efficiency of the disperse textile dye 2-(4-amino-2-nitrophenyl)-1,3-benzothiazole under the experimental conditions evaluated. The higher photocatalyst concentration accelerated dye discoloration and promoted a faster reduction in chemical oxygen demand (COD), indicating an overall improvement in treatment performance. This behavior is consistent with previous studies [10,48], which reported that increasing catalyst loading, within an appropriate range, can enhance photocatalytic activity by increasing the availability of photoactive surface sites and promoting the generation of reactive species involved in pollutant oxidation.

Increasing photocatalyst concentration generally increases the available photoactive surface area and, consequently, the number of sites capable of absorbing radiation and generating electron–hole pairs. Herrmann [49] indicated that photocatalytic degradation rates may increase with catalyst loading until an optimum concentration is reached. However, this trend cannot be extrapolated indefinitely because excessive TiO_2 loading may increase turbidity, particle aggregation, light scattering, and optical shielding, thereby reducing the effective penetration of radiation into the reaction medium [10,21,27,50,51]. Therefore, 400 ppm should be regarded as the best-performing TiO_2 concentration within the range evaluated in this study, rather than as a universal optimum.

The high chemical stability of 2-(4-amino-2-nitrophenyl)-1,3-benzothiazole, associated with its aromatic structure and the presence of amino and nitro groups, as well as the benzothiazole ring, may require sufficient availability of reactive oxidizing species to promote molecular degradation. Rafiq et al. [52] noted that the chemical nature of the pollutant is a determining factor in photocatalytic efficiency, while Hoffmann et al. [18], Fujishima et al. [19], and Schneider et al. [20] described TiO_2 photocatalytic activity in terms of the generation of electron–hole pairs and reactive oxygen species capable of attacking aromatic structures. In this context, the better performance obtained with 400 ppm may be associated with the greater availability of photoactive surface sites and enhanced generation of oxidizing species, without implying direct experimental confirmation of this specific mechanism in the present study.

Overall, the results indicate that TiO_2 concentration is an important operating variable in the photocatalytic process. Within the evaluated range of 200–400 ppm, increasing TiO_2 loading favored dye degradation, which may be associated with a greater availability of photoactive surface area. However, because reactive species were not directly quantified, this explanation should be regarded as a mechanistic interpretation rather than an experimentally demonstrated mechanism. Furthermore, the literature indicates that higher TiO_2 concentrations can lead to light scattering, increased opacity, and particle agglomeration; therefore, extrapolation of these results to higher TiO_2 loadings requires specific experimental verification [21,49–51].

4.2. Influence of pH on the Photocatalytic Process

Solution pH was one of the most influential operating variables affecting the photocatalytic degradation of 2-(4-amino-2-nitrophenyl)-1,3-benzothiazole, simultaneously affecting dye decolorization and chemical oxygen demand (COD) reduction. The highest photocatalytic efficiency was achieved under slightly alkaline conditions (pH 8–9), whereas the lowest performance occurred near pH 6. These observations suggest that pH influences the reaction medium and TiO_2 surface properties, potentially affecting suspension stability and the formation and availability of reactive species involved in dye oxidation, consistent with the decolorization and COD evolution presented in Tables A1–A4.

The observed behavior can be interpreted in relation to the experimentally determined point of zero charge of TiO_2 P25 (pHpzc = 6.2). Under conditions close to pHpzc, the photocatalyst surface has approximately zero net charge, which may reduce electrostatic repulsion between particles and favor aggregation through van der Waals attractive forces. As a consequence, aggregation may decrease the effective surface area available for interfacial processes and increase optical shielding, potentially contributing to the lower photocatalytic efficiency observed near pH 6 [53]. This interpretation is consistent with Derjaguin–Landau–Verwey–Overbeek (DLVO) theory, according to which colloidal stability depends on the balance between attractive and repulsive forces within a suspension.

When pH increases above pHpzc, the surface hydroxyl groups of TiO_2 undergo deprotonation, resulting in a predominantly negatively charged surface. This increased surface charge may enhance electrostatic stabilization of the suspension and reduce particle agglomeration. Greater particle dispersion could promote a more homogeneous distribution of TiO_2 and improve the availability of photoactive surface sites. This behavior has been described by Reza et al. [48] and Hotze et al. [54], who reported the importance of colloidal stability in photocatalytic systems. Similarly, Carrasco-Venegas et al. [55] observed that conditions favoring TiO_2 dispersion can increase the availability of active sites and the overall efficiency of the photocatalytic process. In the present study, these mechanisms provide a plausible explanation for the improved performance observed at pH 9, where the highest decolorization and lowest final COD values were obtained.

In addition to modifying the colloidal stability of the system, pH can influence the surface chemistry of TiO_2 and the generation of reactive oxygen species. Under alkaline conditions, surface hydroxyl groups may participate in reactions with photogenerated holes, contributing to the formation of hydroxyl radicals (•OH), which are important oxidizing species in TiO_2 photocatalysis [19,20,25]. Konstantinou and Albanis [40] reported that the efficiency of photocatalytic dye degradation depends on the generation of reactive oxygen species, the chemical nature of the pollutant, and the pH of the medium, because pH can affect both adsorption and surface oxidation processes. Kisch [56] emphasized that TiO_2 activity depends on interactions among semiconductor surface properties, contaminant adsorption, and electron-transfer pathways during irradiation. Similarly, Kabir Suhan et al. [26] indicated that pH is an important operating variable in TiO_2-based photocatalytic processes because of its influence on catalyst surface charge, pollutant adsorption and oxidizing species generation. Although hydroxyl radicals and other reactive species were not experimentally quantified in the present study, the enhanced decolorization and COD reduction observed at pH 9 are consistent with mechanisms commonly proposed for heterogeneous TiO_2 photocatalysis. In addition, the possible influence of dye acid–base speciation on its affinity for the TiO_2 surface remains a plausible hypothesis that requires further investigation through acid–base equilibrium and pH-dependent adsorption studies [20,41].

From an applied perspective, the pH range of 8–9 associated with the best performance in this study may offer a practical advantage for treating textile effluents that already exhibit slightly alkaline conditions due to the use of chemical auxiliaries during synthetic-fiber dyeing. Consequently, operation at pH 8–9 could reduce the need for extensive pH adjustment. However, this potential advantage must be verified using real effluents because their pH, alkalinity, salinity, and auxiliary chemical composition may differ substantially from the synthetic matrix evaluated in the present study [23]. Crini and Lichtfouse [43] and Jari et al. [27] pointed out that photocatalytic processes may be implemented as advanced or polishing treatments and may require complementary operations, such as TiO_2 recovery, solid–liquid separation, filtration, or subsequent biological treatment before final discharge. Similarly, Kumar and Chowdhury [57] discussed the importance of pH adjustment in optimizing photocatalytic treatment performance. These considerations support further evaluation of the proposed system using real textile wastewater.

Overall, the results indicate that pH plays an important role in photocatalytic performance. Within the investigated range, slightly alkaline conditions provided the most favorable experimental conditions for dye degradation and COD reduction, whereas operation near the TiO_2 point of zero charge resulted in lower photocatalytic efficiency. The observed behavior is consistent with the influence of pH on TiO_2 surface charge and colloidal stability reported for heterogeneous photocatalytic systems; however, the specific contributions of particle aggregation, reactive oxygen species generation, and photocatalyst–pollutant interactions were not directly quantified in this study [10].

4.3. Influence of the Aeration Process on Photocatalytic Degradation

The comparison between experiments performed with and without continuous aeration showed that aeration enhanced the photocatalytic degradation of 2-(4-amino-2-nitrophenyl)-1,3-benzothiazole at both TiO_2 concentrations evaluated. As shown in Tables A1–A4, continuous aeration accelerated dye decolorization and increased chemical oxygen demand (COD) reduction. These results are consistent with the established role of dissolved molecular oxygen as an electron acceptor in TiO_2 photocatalysis and suggest that increased oxygen availability contributed to the improved photocatalytic performance.

Under solar irradiation, TiO_2 absorbs photons with energies equal to or greater than its bandgap energy, promoting electrons from the valence band to the conduction band

and generating electron–hole pairs (e^-/h^+). In the absence of a suitable electron acceptor, these pairs may recombine, dissipating absorbed energy and reducing photocatalytic efficiency. Gerischer and Heller [58] reported that molecular oxygen acts as an important electron acceptor in TiO_2 photocatalytic systems, capturing photogenerated electrons and decreasing the probability of electron–hole recombination. As a result, photogenerated holes can remain available to participate in oxidation reactions at the semiconductor surface, potentially increasing the overall efficiency of the process.

The transfer of electrons to dissolved oxygen can lead to the formation of superoxide radicals ($O_2\bullet^-$), while photogenerated holes can react with water molecules or adsorbed hydroxyl groups to produce hydroxyl radicals (•OH). Hoffmann et al. [18], Fujishima et al. [19], Schneider et al. [20], and Nosaka and Nosaka [25] described these pathways in heterogeneous TiO_2 photocatalysis. Likewise, photogenerated holes may directly oxidize organic molecules adsorbed on the TiO_2 surface through interfacial electron transfer. Thus, dye degradation may proceed through both reactive-oxygen-species-mediated pathways and direct oxidation by photogenerated holes. However, these pathways were not individually quantified in the present study.

Although superoxide radicals participate in oxygen reduction reactions and the formation of secondary reactive species, the specific contributions of individual reactive species to the degradation of 2-(4-amino-2-nitrophenyl)-1,3-benzothiazole cannot be established from the present experimental data. The literature indicates that hydroxyl radicals, superoxide-derived species, and photogenerated holes may contribute to photocatalytic oxidation through different pathways [20,25,41,59].

The availability of dissolved oxygen may become particularly relevant at higher photocatalyst loadings. As the amount of TiO_2 increases, the number of available photoactive sites and, potentially, the number of photogenerated charge carriers may also increase. Schneider et al. [20], Qian et al. [60], Kohtani et al. [61], and Lettieri et al. [62] have discussed the importance of electron transfer to oxygen in limiting electron–hole recombination in TiO_2 photocatalytic systems. Therefore, continuous aeration in the present study likely increased oxygen availability in the reaction medium, which may have contributed to the improved photocatalytic performance.

The results suggest a combined beneficial effect of TiO_2 concentration and aeration. Increasing photocatalyst concentration provides a greater photoactive surface area, whereas aeration can enhance oxygen transfer to the reaction medium. Malato et al. [13] highlighted the importance of oxygen availability in photocatalytic systems. Consequently, the combination of 400 ppm TiO_2 with continuous aeration provided the best photocatalytic performance among the conditions evaluated, resulting in enhanced dye degradation throughout the experimental period.

Overall, continuous aeration enhanced photocatalytic performance, most likely by improving oxygen availability and gas–liquid mixing. Under the investigated conditions, the combination of continuous aeration and 400 ppm TiO_2 produced the highest decolorization and COD reduction, consistent with the beneficial role of oxygen availability reported for TiO_2-based heterogeneous photocatalysis [13,18–20,63–66].

4.4. Interpretation of the Kinetic Behavior of the Photocatalytic Process

The experimental data obtained under the different operating conditions were fitted using pseudo-first-order (PFO) and pseudo-second-order (PSO) kinetic models. Overall, the PSO model provided an adequate empirical description of the temporal evolution of the process, although the best-fitting model varied among experimental conditions. Therefore, the PSO model can be regarded as an empirical representation of the overall dye-removal kinetics rather than evidence of a specific rate-controlling mechanism.

The pseudo-second-order model proposed by Ho and McKay [30] has been widely used to describe adsorption processes and heterogeneous systems involving surface interactions. However, several authors have pointed out that a good statistical fit does not by itself demonstrate the molecular mechanism responsible for the process. Simonin [31] emphasized that empirical kinetic models can adequately describe the temporal evolution of experimental data but should not automatically be interpreted as evidence of a specific adsorption or mass-transfer mechanism. Consequently, a good fit to the PSO model should be interpreted as an empirical description of the overall kinetic behavior rather than evidence that chemisorption controls the photocatalytic process.

In heterogeneous photocatalytic systems, the overall rate results from the simultaneous interaction of several phenomena, including contaminant adsorption on the TiO_2 surface, radiation absorption by the semiconductor, electron–hole pair generation, the formation of reactive oxygen species, and oxidation reactions occurring at the catalyst surface. Therefore, fitting the PSO model may represent the combined contribution of these processes rather than adsorption alone. Ho and McKay [30], Kajjumba et al. [32], and Tran et al. [34] have discussed the application of empirical kinetic models to heterogeneous systems involving multiple surface processes. This interpretation is particularly appropriate for the present study, in which photocatalysis and adsorption may occur simultaneously during treatment.

The fitted kinetic parameters varied with pH and TiO_2 concentration, indicating that the apparent kinetic behavior was influenced by both operating variables. Under alkaline conditions, the observed increase in the apparent reaction rate may be associated with changes in TiO_2 surface properties and colloidal stability, while increasing the photocatalyst concentration may increase the photoactive surface area available for adsorption and photocatalytic reactions. Therefore, the kinetic constants obtained should be regarded as apparent parameters that integrate the combined effects of adsorption, photocatalysis, and operating conditions rather than as intrinsic kinetic constants of the photocatalytic material.

The statistical fit of the PSO model alone does not provide sufficient evidence to identify a specific rate-controlling mechanism or to establish the relative contribution of dye–TiO_2 surface interactions. The results therefore do not demonstrate that surface adsorption controls the overall rate of the process, since photocatalytic performance may also depend on solar irradiation, oxygen availability, pH, photocatalyst concentration, and the generation of reactive oxygen species. This interpretation is consistent with the fundamentals of heterogeneous photocatalysis described by Hoffmann et al. [18], Fujishima et al. [19], and Schneider et al. [20], who described photocatalytic performance as resulting from the interaction of multiple photochemical and interfacial processes.

Overall, the pseudo-second-order model provided a generally adequate empirical description of the photocatalytic process. Nevertheless, the comparative analysis showed that the PFO, Elovich, and Weber–Morris models provided comparable or slightly better fits under certain experimental conditions, as shown in Tables A5–A9. Consequently, the PSO model should be considered an empirical tool for describing the kinetic behavior of the system rather than evidence of a specific reaction mechanism. Identification of the elementary reaction mechanism would require additional experimental approaches, such as dedicated adsorption studies, reactive-species characterization, and the identification of degradation intermediates.

4.5. Mechanism of Oxidation and Partial Mineralization of the Dye

The experimental results indicate that dye removal was not attributable solely to surface adsorption on TiO_2, as both decolorization and a decrease in chemical oxygen demand (COD) were observed during treatment. While decolorization reflects changes in the chromophoric structures responsible for visible-light absorption, COD reduction provides evidence of the progressive oxidation of organic matter in the reaction medium.

Therefore, the joint evaluation of both parameters provides stronger evidence of photocatalytic treatment performance than decolorization alone. Tables A1–A4 show that the greatest COD reductions were generally associated with the conditions that produced the highest decolorization, particularly at 400 ppm TiO_2 with continuous aeration and under alkaline pH conditions, indicating the combined beneficial effects of these operating variables on treatment performance.

The disappearance of color does not necessarily imply complete mineralization of the contaminant. Aromatic dyes may undergo disruption of their chromophoric structures and become colorless, while intermediate organic compounds remain in the reaction medium. Hoffmann et al. [18], Fujishima et al. [19], Schneider et al. [20], and Nosaka and Nosaka [25] described photocatalytic degradation as a sequence of oxidation reactions that can progressively generate lower-molecular-weight intermediates and, under favorable conditions, ultimately lead to CO_2, H_2O, and inorganic ions. Consequently, the decrease in COD observed in the present study should be interpreted as evidence of progressive oxidation and possible partial mineralization rather than complete mineralization, since the final reaction products were not experimentally identified.

Based on the experimental results and established mechanisms reported for heterogeneous photocatalysis, Figure 14 presents a proposed conceptual mechanism for the degradation of 2-(4-amino-2-nitrophenyl)-1,3-benzothiazole. The figure integrates the experimental observations from this study with mechanisms reported in the scientific literature and should therefore be interpreted as a mechanistic hypothesis rather than direct experimental evidence of each reaction pathway represented. The proposed mechanism begins with the absorption of solar radiation by TiO_2 and the generation of electron–hole pairs (e^-/h^+). Photogenerated electrons may be transferred to molecular oxygen, leading to the formation of superoxide radicals ($O_2\bullet^-$), while photogenerated holes may react with water molecules or surface hydroxyl groups to generate hydroxyl radicals (•OH). At the same time, photogenerated holes may directly oxidize dye molecules adsorbed on the TiO_2 surface through interfacial electron transfer. These oxidative pathways provide a plausible mechanistic framework for interpreting the observed dye degradation, although their individual contributions were not experimentally determined in the present study. This interpretation is consistent with mechanisms reported by Hoffmann et al. [18], Fujishima et al. [19], Schneider et al. [20], Nosaka and Nosaka [25], Karimova et al. [41], and Chowdhury et al. [59].

It is important to note that Figure 14 is not intended to establish the quantitative contribution of each reactive species or to experimentally demonstrate the exact sequence of reactions involved in dye degradation. The results provide evidence of photocatalytic oxidation of organic matter; however, they do not allow the individual contributions of hydroxyl radicals, superoxide radicals, or photogenerated holes to be experimentally determined at each stage of the process. Consequently, the proposed mechanism should be understood as a scientifically supported interpretation based on the simultaneous evolution of decolorization and COD, together with established principles of heterogeneous photocatalysis. Accordingly, the specific roles of superoxide radicals, photogenerated holes, and other reactive species should be regarded as mechanistic hypotheses requiring further experimental verification.

Comparison with the recent literature is limited because no peer-reviewed studies were identified that specifically investigated the degradation of 2-(4-amino-2-nitrophenyl)-1,3-benzothiazole using advanced oxidation processes. Therefore, the comparison was extended to studies on benzothiazole (BTH), which contains the same benzothiazole heteroaromatic core. Lai et al. [66] reported BTH degradation using a UV/persulfate process and subsequently demonstrated its effective removal using a UV/peracetic acid system. More recently, Chen et al. [63] compared UV/$K_2S_2O_8$ and UV/H_2O_2 systems, reporting complete and approximately 85% BTH removal, respectively, while Chen et al. [64] achieved

approximately 90% degradation using electron-beam irradiation. Although these studies demonstrate the susceptibility of benzothiazole-based compounds to different advanced oxidation processes, direct comparison with the present study requires caution because of differences in molecular structure, initial pollutant concentrations, irradiation sources, and operating conditions. In contrast, the present study investigated a structurally more complex benzothiazole disperse dye at an initial concentration of 200 mg/L using TiO_2 P25 under natural solar irradiation without external oxidant addition, while simultaneously assessing dye degradation and COD reduction across different pH values, photocatalyst loadings, and aeration conditions. These differences provide a relevant context for interpreting the contribution and scope of the present study.

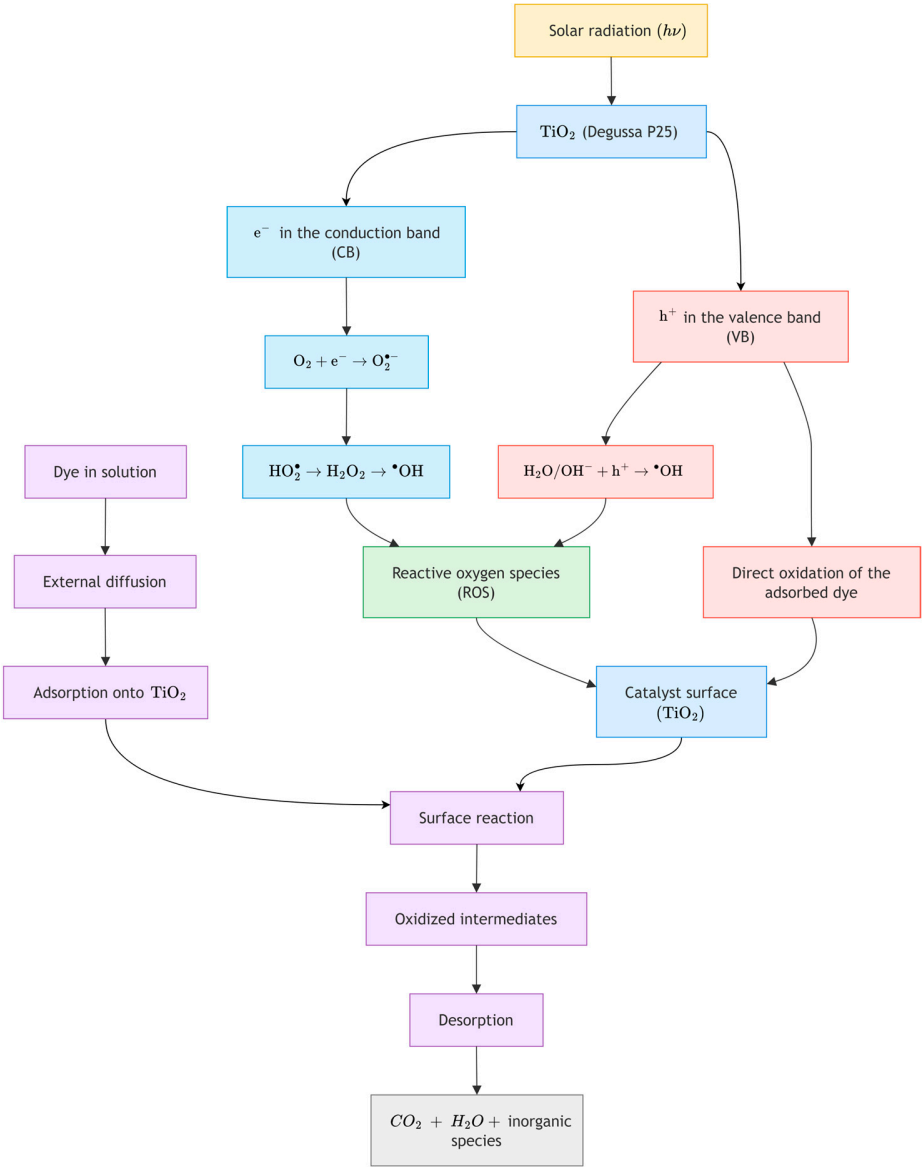

Figure 14. Proposed mechanism of photocatalytic oxidation and partial mineralization of 2-(4-amino-2-nitrophenyl)-1,3-benzothiazole over TiO_2; under solar irradiation.

4.6. Environmental Implications, Application Potential and Constraints

The simultaneous reduction in absorbance and chemical oxygen demand (COD) indicates that the treatment involved not only dye decolorization but also progressive oxidation of organic matter. While absorbance reduction reflects changes in the chromophoric structures responsible for visible-light absorption, COD reduction provides evidence of

organic matter oxidation and possible partial mineralization, since decolorization alone does not necessarily indicate complete degradation of aromatic dyes. This interpretation is consistent with previous studies on TiO_2-based photocatalytic degradation of aromatic compounds [37]. In addition, Karimova et al. [41] highlighted the role of heterogeneous photocatalysis in promoting the oxidation of persistent aromatic structures, whereas Jari et al. [27] emphasized the applicability of photocatalytic processes to textile wastewater treatment. Crini and Lichtfouse [43] further pointed out that the combined evaluation of spectrophotometric indicators and global parameters such as COD provides a more reliable assessment of advanced oxidation processes applied to complex wastewaters. Accordingly, the methodology adopted in the present study helps distinguish chromophore degradation from the progressive oxidation of organic matter, providing stronger evidence of photocatalytic treatment performance than decolorization alone.

Figure 14 provides a conceptual mechanistic interpretation of the degradation pathway of 2-(4-amino-2-nitrophenyl)-1,3-benzothiazole based on the experimental observations and established principles of heterogeneous photocatalysis. As discussed above, this mechanism should not be interpreted as a direct experimental confirmation of individual reaction steps. Definitive identification of degradation intermediates and the contributions of specific reactive species will require complementary analyses, including chromatographic and mass-spectrometric techniques and selective radical scavenging experiments.

Solar TiO_2 photocatalysis may represent an attractive alternative for the treatment of textile effluents containing persistent disperse dyes because it uses solar radiation as the primary energy source, thereby reducing dependence on conventional artificial UV lamps and potentially reducing the external energy demand associated with irradiation. Under the experimental conditions evaluated, the combination of solar irradiation, continuous aeration, and TiO_2 achieved high dye removal efficiencies together with substantial COD reduction, supporting further investigation of this approach for the oxidation of recalcitrant aromatic compounds. In this context, Crini and Lichtfouse [43] highlighted advanced oxidation processes as promising technologies for the treatment of emerging pollutants and complex industrial wastewaters because of their high oxidation capacity and compatibility with conventional treatment processes.

From an operational perspective, the best-performing conditions within the experimental range present potential advantages for further process development. The highest photocatalytic efficiency was achieved using 400 ppm TiO_2, continuous aeration, and slightly alkaline pH. Because some textile effluents may already exhibit alkaline conditions, the extent of pH adjustment required could potentially be reduced; however, this advantage must be confirmed using real wastewater matrices. Solar photocatalysis could therefore be further evaluated as a tertiary or polishing stage within conventional textile wastewater treatment trains, particularly for the removal of residual color and persistent organic compounds [27,37,41].

However, large-scale implementation of the proposed process requires consideration of several additional factors. One of the main challenges is the recovery and reuse of suspended TiO_2 after treatment to prevent nanoparticle release into the environment and reduce operating costs. In addition, process performance may be affected by the composition of real textile wastewater, including dissolved salts, other organic compounds, and chemical auxiliaries that are capable of competing for photocatalyst active sites or affecting light penetration. Consequently, process scale-up should consider complementary strategies such as solid–liquid separation, TiO_2 immobilization on suitable supports, or reactor configurations that facilitate catalyst recovery, as widely discussed in studies of environmental photocatalysis [27,41,43].

An additional limitation of the present study is the absence of experimental identification of degradation intermediates and individual reactive species contributing to the photocatalytic process. Although the combined decrease in absorbance and chemical oxy-

gen demand (COD) provides evidence of progressive dye oxidation, definitive confirmation of the degradation pathway will require complementary studies based on chromatographic techniques, mass spectrometry, and selective radical scavenging experiments. Future research should also evaluate the performance of the proposed system using real textile wastewater, where complex mixtures of dyes, salts, surfactants, and other constituents may influence photocatalytic efficiency under practical operating conditions.

Overall, the results indicate that solar TiO_2 photocatalysis is a promising approach for further investigation in the treatment of textile effluents containing persistent disperse dyes. Under the operating conditions evaluated, the process achieved substantial dye degradation together with COD reduction, supporting its potential application as a solar-driven polishing treatment for textile wastewater. Nevertheless, further studies addressing catalyst recovery, reactor scale-up, treatment of real textile wastewater, and the identification of degradation intermediates and reactive species are essential before the feasibility of industrial implementation can be established.

5. Conclusions

Solar heterogeneous photocatalysis using titanium dioxide (TiO_2) was effective in promoting the degradation of the disperse textile dye 2-(4-amino-2-nitrophenyl)-1,3-benzothiazole under the experimental conditions evaluated. Among the conditions tested, the combination of 400 ppm TiO_2 and continuous aeration provided the highest photocatalytic performance, indicating that photocatalyst concentration and aeration are important operating variables influencing process efficiency.

The pH exerted a significant influence on treatment efficiency. The highest dye degradation rates and greatest reductions in chemical oxygen demand (COD) were obtained under slightly alkaline conditions (pH 8–9), while the lowest photocatalytic performance was observed near the TiO_2 point of zero charge (pHpzc $\approx$ 6.2). This behavior may be associated with pH-dependent changes in TiO_2 surface charge and colloidal stability, which can affect nanoparticle dispersion, surface-site availability, and overall photocatalytic performance.

The pseudo-second-order kinetic model generally provided an adequate empirical description of the experimental data. Nevertheless, the comparative analysis showed that the model providing the best statistical fit varied among the experimental conditions evaluated. These empirical fits should be interpreted as mathematical descriptions of the overall process, reflecting the combined influences of surface adsorption, photooxidation, and operating conditions, rather than as evidence of a specific rate-controlling mechanism.

The simultaneous decrease in dye concentration and chemical oxygen demand indicated that the treatment resulted not only in decolorization but also in the progressive oxidation of organic matter. However, COD reduction should be interpreted as evidence of progressive oxidation and possible partial mineralization rather than complete mineralization, because degradation intermediates and final products were not experimentally identified. In this context, the mechanism proposed in Figure 14 should be regarded as a conceptual interpretation integrating the experimental observations with established principles of heterogeneous photocatalysis rather than as direct experimental evidence of the individual reactive species or elementary reaction steps involved in dye degradation.

The integration of kinetic analysis with the simultaneous evaluation of decolorization and COD provided a more comprehensive interpretation of the overall dye-removal process and helped distinguish apparent adsorption-related behavior from photocatalytic oxidation. Likewise, solar irradiation combined with 400 ppm TiO_2, continuous aeration, and slightly alkaline conditions provided the best treatment performance within the experimental range investigated. These findings provide laboratory-scale evidence that can support further optimization of solar photocatalytic treatment systems for persistent aromatic dyes.

Together, the findings obtained not only expand knowledge about the photocatalytic degradation of benzothiazole disperse dyes under solar irradiation, but also provide experimental criteria for the optimization of operational variables and for the future scaling of photocatalytic systems for the treatment of textile effluents. This work contributes to the development of more efficient advanced oxidation technologies based on solar photocatalysis and provides experimental information that may support future research aimed at developing solar-driven wastewater treatment systems with reduced dependence on artificial UV irradiation.

Finally, future research should be oriented towards the identification of degradation intermediates, the evaluation of the toxicity of the treated effluents, the recovery and reuse of the photocatalyst, the study of the process using real textile effluents, and the design of reactors that facilitate the industrial scale-up of this technology.

Author Contributions: Conceptualization, L.A.C.-V.; methodology, D.G.M.-H. and L.A.C.-V.; software, J.T.M.-C. and R.P.-S.; validation, C.G.-C. and H.R.C.-T.; formal analysis, J.T.M.-C.; investigation, L.A.C.-V., F.O.-B. and H.R.C.-T.; resources, S.T.P. and L.A.C.-V.; data curation, D.G.M.-H. and C.G.-C.; writing—original draft preparation, L.A.C.-V.; writing—review and editing, J.T.M.-C. and L.A.C.-V.; supervision, L.G.C.-P. and C.G.-C.; project administration, J.T.M.-C.; funding acquisition, L.A.C.-V. and R.P.-S. All authors have read and agreed to the published version of the manuscript.

Funding: This research was funded by Universidad Nacional del Callao, Lima, Peru.

Data Availability Statement: The original contributions of this study are included in the article. For further information, please contact the corresponding author.

Acknowledgments: The authors would like to thank the Universidad Nacional del Callao (Peru) for providing financial support for the publication of this article. The authors gratefully acknowledge Gloria Contreras Caballón, General Manager of SOQUITEX ING S.R.L., for her valuable support in providing the disperse textile dye 2-(4-amino-2-nitrophenyl)-1,3-benzothiazole used in the experimental work of this study.

Conflicts of Interest: The authors declare no conflicts of interest.

Appendix A

Table A1. Dye concentration as a function of time, with aeration and 200 ppm TiO_2 nanoparticles, expressed in terms of color change.

t (h)	pH				
	5	6	7	8	9
	C (mg/L)	C (mg/L)	C (mg/L)	C (mg/L)	C (mg/L)
0	200	200	200	200	200
12	167.2 ± 0.47	180.1 ± 0.39	154.5 ± 0.12	128.3 ± 0.92	90.4 ± 1
23.5	141.5 ± 0.06	169.8 ± 0.8	128.4 ± 0.25	82.3 ± 0.98	45.1 ± 0.49
40	108.1 ± 0.51	154.1 ± 0.82	96.8 ± 0.83	45.5 ± 0.57	15.4 ± 0.91
50	99.4 ± 0.31	146.2 ± 0.92	82.5 ± 0.45	38.2 ± 0.74	8.9 ± 0.68
60	88.3 ± 0.55	135.1 ± 0.82	68.3 ± 0.12	28.6 ± 0.27	4.8 ± 0.69
70	78.5 ± 0.05	132.8 ± 0.18	61.4 ± 0.36	19.6 ± 0.25	2.7 ± 0.32
83.5	65.2 ± 0.05	125.4 ± 0.88	51.2 ± 0.02	15 ± 0.92	1.1 ± 0.64
100	58.1 ± 0.38	112.6 ± 0.24	39.5 ± 0.3	9.8 ± 0.8	0.4 ± 0.09
108	53.8 ± 0.53	114.2 ± 0.51	37.6 ± 0.78	7.1 ± 0.28	0.2 ± 0.05
130	42.5 ± 0.69	108.1 ± 0.7	25.1 ± 0.36	4.2 ± 0.67	-
154.5	36.4 ± 0.27	98.5 ± 0.21	22.3 ± 0.32	3.1 ± 0.14	-
Final COD (mg/L)	83.2 ± 0.77	220.4 ± 0.49	52.7 ± 0.64	12.3 ± 0.62	5.3 ± 0.96

Table A2. Dye concentration as a function of time, without aeration and with 200 ppm of TiO_2 nanoparticles, expressed in terms of color change.

t (h)	pH				
	5	6	7	8	9
	C (mg/L)	C (mg/L)	C (mg/L)	C (mg/L)	C (mg/L)
0	200	200	200	200	200
12	190.4 ± 0.96	196.5 ± 0.49	191.2 ± 0.54	188.4 ± 1.3	186.2 ± 0.48
23.5	188.5 ± 0.26	194.2 ± 0.43	184.6 ± 0.40	182.2 ± 0.4	179.8 ± 0.60
40	184.1 ± 0.82	192.8 ± 0.87	181.1 ± 0.60	175.3 ± 0.19	172.1 ± 0.15
50	181.7 ± 0.51	190.2 ± 0.54	177.9 ± 0.79	170.8 ± 0.96	167.4 ± 0.45
60	179.8 ± 0.99	189.1 ± 0.2	175.4 ± 0.91	167.2 ± 0.28	163.5 ± 0.95
70	177.9 ± 0.11	188.3 ± 0.91	173.2 ± 0.82	164.5 ± 0.56	160.2 ± 0.29
83.5	175.8 ± 0.34	187.3 ± 0.07	171.8 ± 0.19	162.6 ± 0.46	156.8 ± 0.63
100	173.7 ± 0.57	186.2 ± 0.17	168.4 ± 0.85	158.8 ± 0.51	153.6 ± 0.79
108	172.9 ± 0.68	185.1 ± 0.86	167.3 ± 0.94	157.6 ± 0.16	152.3 ± 0.75
130	171.1 ± 0.24	184.8 ± 0.62	164.9 ± 0.32	155 ± 0.87	147.3 ± 0.45
154.5	165.4 ± 0.51	181.8 ± 0.15	161.3 ± 0.78	150.8 ± 0.52	144.1 ± 0.51
Final COD (mg/L)	382.3 ± 0.77	390.3 ± 0.49	370.43 ± 0.64	365.9 ± 0.62	340.2 ± 0.96

Table A3. Dye concentration as a function of time, with aeration and 400 ppm TiO_2 nanoparticles, expressed in terms of color change.

t (h)	pH				
	5	6	7	8	9
	C (mg/L)	C (mg/L)	C (mg/L)	C (mg/L)	C (mg/L)
0	200	200	200	200	200
10	170 ± 0.33	154.2 ± 0.80	163.5 ± 0.87	141.2 ± 0.46	100.4 ± 0.64
20	142 ± 0.81	128.9 ± 0.8	145.6 ± 0.56	89.7 ± 0.56	42.4 ± 0.06
30.5	130 ± 0.51	90.3 ± 0.09	129.8 ± 0.15	69.1 ± 0.7	27.7 ± 0.17
40.2	98 ± 0.91	75.3 ± 0.52	113.1 ± 0.21	54.3 ± 0.46	13.5 ± 0.33
50	74 ± 0.57	54.5 ± 0.73	90.4 ± 0.68	35.1 ± 0.96	7.8 ± 0.18
60.5	60 ± 0.62	41.5 ± 0.55	84.8 ± 0.71	20.4 ± 0.91	2.4 ± 0.73
70	47 ± 0.67	32.4 ± 0.87	74.1 ± 0.66	17.5 ± 0.8	1.1 ± 0.51
Final COD (mg/L)	75.5 ± 0.77	178.8 ± 0.49	40.2 ± 0.64	7.3 ± 0.62	2.4 ± 0.96

Table A4. Dye concentration as a function of time, without aeration and with 400 ppm of TiO_2 nanoparticles, expressed in terms of color change.

t (h)	pH				
	5	6	7	8	9
	C (mg/L)	C (mg/L)	C (mg/L)	C (mg/L)	C (mg/L)
0	200	200	200	200	200
10	188.5 ± 1.08	192.2 ± 0.86	185.1 ± 1.29	179.4 ± 0.75	173.8 ± 0.92
20	181.2 ± 0.12	190.1 ± 0.29	177.4 ± 0.97	167.2 ± 0.24	160.4 ± 0.42
30.5	175.4 ± 0.34	186.3 ± 0.6	167.9 ± 0.32	154.8 ± 0.53	150.9 ± 0.83
40.2	172.4 ± 0.12	185.1 ± 0.4	163.4 ± 0.67	147.2 ± 0.41	140.4 ± 0.58
50	166.4 ± 0.14	182.5 ± 0.42	155.8 ± 0.56	143.2 ± 0.81	133.4 ± 0.52
60.5	164.1 ± 0.42	181.6 ± 0.74	153.9 ± 0.66	135.9 ± 0.52	129.3 ± 0.56
70	160.5 ± 0.83	178.9 ± 0.06	150.8 ± 0.87	131.8 ± 0.50	122.4 ± 0.09
Final COD (mg/L)	360.5 ± 0.77	388.2 ± 0.89	345.5 ± 0.64	320.3 ± 0.62	312.7 ± 0.96

Table A5. Kinetic models evaluated.

Model	Equation	Parameters	Reference
PFO	$\frac{dq_t}{dt} = k_1(q_e - q_t)$	$(q_e;\ k_1)$	Lagergren [45]
PSO	$\frac{dq_t}{dt} = k_2(q_e - q_t)^2$	$(q_e;\ k_2)$	Ho & McKay [30]
Elovich	$q_t = \frac{\ln(1+\alpha\beta t)}{\beta}$	$(\alpha;\ \beta)$	Wu et al. [46]
Weber–Morris	$q_t = k_{id}t^{1/2} + C$	$(k_{id};\ C)$	Weber & Morris [47]

The goodness of fit was evaluated using the coefficient of determination (R^2) and the chi-square statistic, calculated as $\chi^2 = \sum_{i=1}^{n} \frac{\left(q_{exp,i} - q_{calc,i}\right)^2}{q_{calc,i}}$. Lower χ^2 values indicate closer agreement between the experimental and model-calculated values.

Table A6. Kinetic fitting parameters for 200 ppm TiO_2 with aeration.

pH	Model	Adjusted Parameters	R^2	X^2
5	PFO	$q_e = 934.1627;\ k_1 = 0.02319$	0.971	228.3127
	PSO	$q_e = 1251.3182;\ k_2 = 1.066 \times 10^{-5}$	0.9936	3.146
	Elovich	$\alpha = 21.2390;\ \beta = 0.002705$	0.9953	9.2963
	Weber–Morris	$k_{id} = 71.7340;\ C = -19.6522$	0.9826	32.4281
6	PFO	$q_e = 548.6478;\ k_1 = 0.01834$	0.9824	61.5378
	PSO	$q_e = 810.4171;\ k_2 = 1.289 \times 10^{-5}$	0.9724	4.2203
	Elovich	$\alpha = 9.2698;\ \beta = 0.003503$	0.9953	4.1004
	Weber–Morris	$k_{id} = 43.7527;\ C = -31.1620$	0.9851	13.4801
7	PFO	$q_e = 1091.9626;\ k_1 = 0.02755$	0.9312	536.4616
	PSO	$q_e = 1243.1237;\ k_2 = 1.447 \times 10^{-5}$	0.9984	1.723
	Elovich	$\alpha = 29.6540;\ \beta = 0.002849$	0.9955	6.6371
	Weber–Morris	$k_{id} = 77.1434;\ C = 10.6611$	0.9803	28.3065
8	PFO	$q_e = 1043.7592;\ k_1 = 0.03702$	0.9848	37.3984
	PSO	$q_e = 1172.2183;\ k_2 = 3.689 \times 10^{-5}$	0.9972	7.831
	Elovich	$\alpha = 99.8553;\ \beta = 0.003891$	0.9785	32.7926
	Weber–Morris	$k_{id} = 80.6999;\ C = 144.4288$	0.8993	99.5392
9	PFO	$q_e = 1096.0959;\ k_1 = 0.06673$	0.995	78.2997
	PSO	$q_e = 1101.5913;\ k_2 = 9.752 \times 10^{-5}$	0.9975	11.5118
	Elovich	$\alpha = 686.3136;\ \beta = 0.005988$	0.9647	33.8038
	Weber–Morris	$k_{id} = 73.4112;\ C = 288.4369$	0.7624	120.7681

Table A7. Kinetic fitting parameters for 200 ppm TiO_2 without aeration.

pH	Model	Adjusted Parameters	R^2	χ^2
5	PFO	$q_e = 177.0411;\ k_1 = 0.0146$	0.9706	16.2892
	PSO	$q_e = 243.4359;\ k_2 = 5.072 \times 10^{-5}$	0.9788	10.5641
	Elovich	$\alpha = 3.7202;\ \beta = 0.0134$	0.9854	6.1606
	Weber–Morris	$k_{id} = 13.4117;\ C = -2.4498$	0.9931	1.6116
6	PFO	$q_e = 99.8458;\ k_1 = 0.0126$	0.9869	2.5096
	PSO	$q_e = 144.3640;\ k_2 = 6.698 \times 10^{-5}$	0.9896	1.7365
	Elovich	$\alpha = 1.5910;\ \beta = 0.0206$	0.9911	1.3103
	Weber–Morris	$k_{id} = 7.4243;\ C = -4.8716$	0.9851	2.0949
7	PFO	$q_e = 200.4112;\ k_1 = 0.0162$	0.9879	5.9949
	PSO	$q_e = 273.3382;\ k_2 = 5.097 \times 10^{-5}$	0.9938	2.6343
	Elovich	$\alpha = 4.7161;\ \beta = 0.0120$	0.9972	1.0267
	Weber–Morris	$k_{id} = 15.8974;\ C = -2.9206$	0.9962	1.7731

Table A7. *Cont.*

pH	Model	Adjusted Parameters	R^2	χ^2
8	PFO	$q_e = 255.7188$; $k_1 = 0.0169$	0.995	3.6097
	PSO	$q_e = 349.5496$; $k_2 = 4.121 \times 10^{-5}$	0.9981	1.2242
	Elovich	$\alpha = 6.1911$; $\beta = 0.009364$	0.9985	0.5984
	Weber–Morris	$k_{id} = 20.6313$; $C = -3.9327$	0.9928	3.3884
9	PFO	$q_e = 295.6859$; $k_1 = 0.0162$	0.9936	6.5951
	PSO	$q_e = 405.9901$; $k_2 = 3.377 \times 10^{-5}$	0.9973	2.755
	Elovich	$\alpha = 6.8189$; $\beta = 0.008016$	0.9988	0.9305
	Weber–Morris	$k_{id} = 23.5218$; $C = -5.1048$	0.9955	2.2826

Table A8. Kinetic fitting parameters for 400 ppm TiO_2 with aeration.

pH	Model	Adjusted Parameters	R^2	χ^2
5	PFO	$q_e = 841.6481$; $k_1 = 0.0392$	0.993	6.15
	PSO	$q_e = 1484.6380$; $k_2 = 3.415 \times 10^{-6}$	0.9929	6.31
	Elovich	$\alpha = 7.6261$; $\beta = 0.001543$	0.9928	6.4
	Weber–Morris	$k_{id} = 48.0862$; $C = -44.5526$	0.9443	49.55
6	PFO	$q_e = 532.2047$; $k_1 = 0.0225$	0.9972	2.76
	PSO	$q_e = 809.6884$; $k_2 = 1.947 \times 10^{-5}$	0.9967	3.35
	Elovich	$\alpha = 13.8294$; $\beta = 0.003414$	0.996	4.09
	Weber–Morris	$k_{id} = 53.1361$; $C = -26.5460$	0.981	18.83
7	PFO	$q_e = 427.2855$; $k_1 = 0.0189$	0.9911	6.51
	PSO	$q_e = 660.5644$; $k_2 = 1.963 \times 10^{-5}$	0.9919	5.53
	Elovich	$\alpha = 9.2353$; $\beta = 0.004115$	0.9926	4.7
	Weber–Morris	$k_{id} = 38.8174$; $C = -20.1585$	0.9781	14.21
8	PFO	$q_e = 492.6936$; $k_1 = 0.0368$	0.9957	5.3
	PSO	$q_e = 673.8705$; $k_2 = 4.623 \times 10^{-5}$	0.9962	4.49
	Elovich	$\alpha = 25.6894$; $\beta = 0.004856$	0.9945	6.28
	Weber–Morris	$k_{id} = 57.5014$; $C = -3.0403$	0.9875	13.51
9	PFO	$q_e = 497.0375$; $k_1 = 0.0719$	0.998	2.51
	PSO	$q_e = 595.9650$; $k_2 = 1.39 \times 10^{-4}$	0.9945	6.47
	Elovich	$\alpha = 102.5191$; $\beta = 0.007762$	0.9853	15.44
	Weber–Morris	$k_{id} = 60.2980$; $C = 54.5282$	0.9267	67.56

Table A9. Kinetic fitting parameters for 400 ppm TiO_2 without aeration.

pH	Model	Adjusted Parameters	R^2	χ^2
5	PFO	$q_e = 118.0587$; $k_1 = 0.0243$	0.9946	1.251
	PSO	$q_e = 173.8477$; $k_2 = 1.04 \times 10^{-4}$	0.9963	0.782
	Elovich	$\alpha = 3.5111$; $\beta = 0.0167$	0.9974	0.521
	Weber–Morris	$k_{id} = 12.0491$; $C = -4.4885$	0.9903	2.163
6	PFO	$q_e = 56.6188$; $k_1 = 0.0303$	0.9798	2.214
	PSO	$q_e = 78.5443$; $k_2 = 3.20 \times 10^{-4}$	0.9851	1.547
	Elovich	$\alpha = 2.4083$; $\beta = 0.0410$	0.9893	1.043
	Weber–Morris	$k_{id} = 6.1591$; $C = -0.6029$	0.9934	0.604
7	PFO	$q_e = 147.9633$; $k_1 = 0.0255$	0.9961	1.286
	PSO	$q_e = 218.1042$; $k_2 = 8.633 \times 10^{-5}$	0.9963	1.104
	Elovich	$\alpha = 4.5877$; $\beta = 0.0133$	0.996	1.209
	Weber–Morris	$k_{id} = 15.4498$; $C = -5.7075$	0.9871	4.087
8	PFO	$q_e = 196.2738$; $k_1 = 0.0277$	0.9978	1.036
	PSO	$q_e = 283.8856$; $k_2 = 7.455 \times 10^{-5}$	0.9987	0.584
	Elovich	$\alpha = 6.8369$; $\beta = 0.0105$	0.9987	0.596
	Weber–Morris	$k_{id} = 21.1235$; $C = -6.3756$	0.992	3.409

Table A9. *Cont.*

pH	Model	Adjusted Parameters	R^2	χ^2
9	PFO	$q_e = 213.9270$; $k_1 = 0.0304$	0.9939	2.977
	PSO	$q_e = 300.6113$; $k_2 = 8.158 \times 10^{-5}$	0.9966	1.554
	Elovich	$\alpha = 8.7485$; $\beta = 0.0104$	0.9982	0.765
	Weber–Morris	$k_{id} = 23.5209$; $C = -3.8944$	0.9968	1.284

References

1. Kant, R. Textile dyeing industry an environmental Hazard. *Nat. Sci.* **2012**, *4*, 22–26. [CrossRef]
2. Yaseen, D.A.; Scholz, M. Textile dye wastewater characteristics and constituents of synthetic effluents: A critical review. *Int. J. Environ. Sci. Technol.* **2019**, *16*, 1193–1226. [CrossRef]
3. Khan, S.; Noor, T.; Iqbal, N.; Yaqoob, L. Photocatalytic Dye Degradation from Textile Wastewater: A Review. *ACS Omega* **2024**, *9*, 21751–21767. [CrossRef] [PubMed]
4. Bopape, D.A.; Ntsendwana, B.; Mabasa, F.D. Photocatalysis as a pre-discharge treatment to improve the effect of textile dyes on human health: A critical review. *Heliyon* **2024**, *10*, e39316. [CrossRef] [PubMed]
5. Hao, O.J.; Kim, H.; Chiang, P.-C. Decolorization of Wastewater. *Crit. Rev. Environ. Sci. Technol.* **2000**, *30*, 449–505. [CrossRef]
6. Saratale, R.G.; Saratale, G.D.; Chang, J.S.; Govindwar, S.P. Decolorization and detoxification of reactive textile dyes by an isolated bacterium. *J. Environ. Manag.* **2011**, *92*, 843–851.
7. Forgacs, E.; Cserháti, T.; Oros, G. Environmental aspects of textile dyeing technologies. *Rev. Environ. Contam. Toxicol.* **2004**, *181*, 65–104.
8. Ben Slama, H.; Bouket, A.C.; Pourhassan, Z.; Alenezi, F.N.; Silini, A.; Cherif-Silini, H.; Oszako, T.; Luptakova, L.; Golińska, P.; Belbahri, L. Diversity of Synthetic Dyes from Textile Industries, Discharge Impacts and Treatment Methods. *Appl. Sci.* **2021**, *11*, 6255. [CrossRef]
9. Kumari, H.; Sonia; Suman; Ranga, R.; Chahal, S.; Devi, S.; Sharma, S.; Kumar, S.; Kumar, P.; Kumar, S.; et al. A Review on Photocatalysis Used For Wastewater Treatment: Dye Degradation. *Water Air Soil Pollut.* **2023**, *234*, 349. [CrossRef] [PubMed]
10. Zaaboul, F.; Canle, M.; Haoufazane, C.; Santaballa, J.A.; Hammouti, B.; Azzaoui, K.; Jodeh, S.; Hadjadj, A.; El Hourch, A. Sunlight-Driven Photodegradation of RB49 Dye Using TiO_2-P25 and TiO_2-UV100: Performance Comparison. *Coatings* **2024**, *14*, 1270. [CrossRef]
11. Zodrow, K.R.; Li, Q.; Buono, R.M.; Chen, W.; Daigger, G.; Dueñas-Osorio, L.; Elimelech, M.; Huang, X.; Jiang, G.; Kim, J.-H.; et al. Advanced Materials, Technologies, and Complex Systems Analyses: Emerging Opportunities to Enhance Urban Water Security. *Environ. Sci. Technol.* **2017**, *51*, 10274–10281. [CrossRef] [PubMed]
12. Zodrow, K.; Padhye, L.P.; Suthar, P. Emerging investigator series: Toxicity and removal of textile dyes in water and wastewater. *Environ. Sci. Water Res. Technol.* **2021**, *7*, 2110–2130.
13. Malato, S.; Fernández-Ibáñez, P.; Maldonado, M.; Blanco, J.; Gernjak, W. Decontamination and disinfection of water by solar photocatalysis: Recent overview and trends. *Catal. Today* **2009**, *147*, 1–59. [CrossRef]
14. Oturan, M.A.; Aaron, J.-J. Advanced Oxidation Processes in Water/Wastewater Treatment: Principles and Applications. A Review. *Crit. Rev. Environ. Sci. Technol.* **2014**, *44*, 2577–2641. [CrossRef]
15. Brillas, E.; Martínez-Huitle, C.A. Decontamination of wastewaters containing synthetic organic dyes by electrochemical methods. An updated review. *Appl. Catal. B Environ. Energy* **2015**, *166–167*, 603–643. [CrossRef]
16. Romero, H.M.Z.; Vázquez, C. Evaluation of the Efficiency of an Electrocoagulation Cell for the Treatment of Wastewater coming from the Textile Industry. In *Proceedings of the 21th LACCEI International Multi-Conference for Engineering, Education and Technology (LACCEI 2023): "Leadership in Education and Innovation in Engineering in the Framework of Global Transformations: Integration and Alliances for Integra"*; Latin American and Caribbean Consortium of Engineering Institutions: Boca Raton, FL, USA, 2023. [CrossRef]
17. França, Y.K.d.S.; Pereira, K.S.; Feitosa, Y.H.C.; Marques, V.B.; de Souza, D.R. Titanium Dioxide (TiO_2) and Photocatalysis: A Detailed Overview of the Synthesis, Applications, Challenges, Advances and Prospects for Sustainable Development. *Orbital Electron. J. Chem.* **2025**, *17*, 355–381. [CrossRef]
18. Hoffmann, M.R.; Martin, S.T.; Choi, W.; Bahnemann, D.W. Environmental Applications of Semiconductor Photocatalysis. *Chem. Rev.* **1995**, *95*, 69–96. [CrossRef]
19. Fujishima, A.; Zhang, X.; Tryk, D.A. TiO_2 photocatalysis and related surface phenomena. *Surf. Sci. Rep.* **2008**, *63*, 515–582. [CrossRef]
20. Schneider, J.; Matsuoka, M.; Takeuchi, M.; Zhang, J.; Horiuchi, Y.; Anpo, M.; Bahnemann, D.W. Understanding TiO_2 Photocatalysis: Mechanisms and Materials. *Chem. Rev.* **2014**, *114*, 9919–9986. [CrossRef] [PubMed]

21. Chong, M.N.; Jin, B.; Chow, C.W.K.; Saint, C. Recent developments in photocatalytic water treatment technology: A review. *Water Res.* **2010**, *44*, 2997–3027. [CrossRef] [PubMed]
22. Haleem, A.; Shafiq, A.; Chen, S.-Q.; Nazar, M. A Comprehensive Review on Adsorption, Photocatalytic and Chemical Degradation of Dyes and Nitro-Compounds over Different Kinds of Porous and Composite Materials. *Molecules* **2023**, *28*, 1081. [CrossRef] [PubMed]
23. Muscetta, M.; Ganguly, P.; Clarizia, L. Solar-powered photocatalysis in water purification: Applications and commercialization challenges. *J. Environ. Chem. Eng.* **2024**, *12*, 113073. [CrossRef]
24. Chen, X.; Mao, S.S. Titanium dioxide nanomaterials: Synthesis, properties, modifications, and applications. *Chem. Rev.* **2007**, *107*, 2891–2959. [CrossRef] [PubMed]
25. Nosaka, Y.; Nosaka, A.Y. Generation and Detection of Reactive Oxygen Species in Photocatalysis. *Chem. Rev.* **2017**, *117*, 11302–11336. [CrossRef] [PubMed]
26. Suhan, B.K.; Al-Mamun, R.; Farzana, N.; Aishee, S.M.; Islam, S.; Marwani, H.M.; Hasan, M.; Asiri, A.M.; Rahman, M.M.; Islam, A.; et al. Sustainable pollutant removal and wastewater remediation using TiO_2-based nanocomposites: A critical review. *Nano-Struct. Nano-Objects* **2023**, *36*, 101050. [CrossRef]
27. Jari, Y.; Najid, N.; Necibi, M.C.; Gourich, B.; Vial, C.; Elhalil, A.; Kaur, P.; Mohdeb, I.; Park, Y.; Hwang, Y.; et al. A comprehensive review on TiO_2-based heterogeneous photocatalytic technologies for emerging pollutants removal from water and wastewater: From engineering aspects to modeling approaches. *J. Environ. Manag.* **2025**, *373*, 123703. [CrossRef] [PubMed]
28. Avargani, V.M.; Zendehboudi, S.; Osfouri, S.; Rostami, A. Performance evaluation of a solar nano-photocatalytic reactor for wastewater treatment applications: Reaction kinetics, CFD, and scale-up perspectives. *J. Clean. Prod.* **2023**, *421*, 138240. [CrossRef]
29. Shokrgozar, A.; Seifpanahi-Shabani, K.; Mahmoodi, B.; Mahmoodi, N.M.; Khorasheh, F.; Baghalha, M. Synthesis of Ni-Co-CNT nanocomposite and evaluation of its photocatalytic dye (Reactive Red 120) degradation ability using response surface methodology. *Desalin. Water Treat.* **2021**, *216*, 389–400. [CrossRef]
30. Ho, Y.S.; McKay, G. Pseudo-second order model for sorption processes. *Process Biochem.* **1999**, *34*, 451–465. [CrossRef]
31. Simonin, J.P. On the comparison of pseudo-first order and pseudo-second order rate laws in the modeling of adsorption kinetics. *Chem. Eng. J.* **2016**, *300*, 254–263. [CrossRef]
32. Kajjumba, G.W.; Emik, S.; Öngen, A.; Özcan, H.K.; Aydın, S. Modelling of Adsorption Kinetic Processes—Errors, Theory and Application. In *Advanced Sorption Process Applications*; IntechOpen: London, UK, 2019. [CrossRef]
33. Pino, E.; Calderón, C.; Castro, P. TiO_2 Photocatalyzed Degradation of the Azo Dye Disperse Red 1 in Aqueous Micellar Environments. *Photochem. Photobiol.* **2021**, *97*, 40–46. [CrossRef] [PubMed]
34. Tran, H.N.; You, S.-J.; Hosseini-Bandegharaei, A.; Chao, H.-P. Mistakes and inconsistencies regarding adsorption of contaminants from aqueous solutions: A critical review. *Water Res.* **2017**, *120*, 88–116. [CrossRef] [PubMed]
35. Azizian, S. Kinetic models of sorption: A theoretical analysis. *J. Colloid Interface Sci.* **2004**, *276*, 47–52. [CrossRef] [PubMed]
36. Suarez-Escobar, A.F.; Conde-Rivera, L.R.; Lopez-Suarez, F.E.; Illán-Gómez, M.J.; Gonzalez-Hernandez, K.S.; Chalapud-Morales, J.S. Heterogeneous Photocatalytic Degradation of Ibuprofen Over TiO_2–Ag Supported on Activated Carbon from Waste Tire Rubber. *Top. Catal.* **2021**, *64*, 51–64. [CrossRef]
37. Rashid, M.K.; Salman, I.R.; Obaid, A.L.; Hassan, S.A.-D.H.; Al-Musawi, M.R.; Al-Saady, M. Application of machine learning in predicting sources of water pollution in the Euphrates and Tigris rivers in Iraq. *Int. J. Aquat. Biol.* **2024**, *12*, 581–589. [CrossRef]
38. Malato, S.; Maldonado, M.I.; Fernández-Ibáñez, P.; Oller, I.; Polo, I.; Sánchez-Moreno, R. Decontamination and Disinfection of Water by Solar Photocatalysis: The Pilot Plants of the Plataforma Solar de Almeria. *Mater. Sci. Semicond. Process.* **2016**, *42*, 15–23. [CrossRef]
39. Ghasemi, A.H.; Zoqi, M.J.; Ranjbar, P.Z. Enhanced photocatalytic degradation of methylene blue using a novel counter-rotating disc reactor. *Front. Chem.* **2024**, *12*, 1335180. [CrossRef] [PubMed]
40. Konstantinou, I.K.; Albanis, T.A. TiO_2-assisted photocatalytic degradation of azo dyes in aqueous solution: Kinetic and mechanistic investigations: A review. *Appl. Catal. B Environ.* **2004**, *49*, 1–14. [CrossRef]
41. Karimova, N.V.; Wang, W.; Gerber, R.B.; Finlayson-Pitts, B.J. Experimental and theoretical investigation of benzothiazole oxidation by OH in air and the role of O_2. *Environ. Sci. Process. Impacts* **2024**, *26*, 2177–2188. [CrossRef] [PubMed]
42. Kane, A.; Assadi, A.A.; El Jery, A.; Badawi, A.K.; Kenfoud, H.; Baaloudj, O.; Assadi, A.A. Advanced Photocatalytic Treatment of Wastewater Using Immobilized Titanium Dioxide as a Photocatalyst in a Pilot-Scale Reactor: Process Intensification. *Materials* **2022**, *15*, 4547. [CrossRef] [PubMed]
43. Crini, G.; Lichtfouse, E. Advantages and disadvantages of techniques used for wastewater treatment. *Environ. Chem. Lett.* **2019**, *17*, 145–155. [CrossRef]
44. Servicio Nacional de Meteorología e Hidrología del Perú. SENAMHI—Radiacion Uv. Available online: https://www.senamhi.gob.pe/?p=radiacion-uv (accessed on 28 January 2026).
45. Lagergren, S. About the theory of so-called adsorption of soluble substances. *K. Sven. Vetenskapsakademiens Handl.* **1898**, *24*, 1–39.

46. Wu, F.-C.; Tseng, R.-L.; Juang, R.-S. Characteristics of Elovich equation used for the analysis of adsorption kinetics in dye-chitosan systems. *Chem. Eng. J.* **2009**, *150*, 366–373. [CrossRef]
47. Weber, W.J.; Morris, J.C. Kinetics of adsorption on carbon from solution. *J. Sanit. Eng. Div.* **1963**, *89*, 31–60. [CrossRef]
48. Reza, K.M.; Kurny, A.S.W.; Gulshan, F. Parameters affecting the photocatalytic degradation of dyes using TiO_2: A review. *Appl. Water Sci.* **2017**, *7*, 1569–1578. [CrossRef]
49. Herrmann, J.-M. Heterogeneous photocatalysis: Fundamentals and applications to the removal of various types of aqueous pollutants. *Catal. Today* **1999**, *53*, 115–129. [CrossRef]
50. Han, F.; Kambala, V.S.R.; Srinivasan, M.; Rajarathnam, D.; Naidu, R. Tailored titanium dioxide photocatalysts for the degradation of organic dyes in wastewater treatment: A review. *Appl. Catal. A Gen.* **2009**, *359*, 25–40. [CrossRef]
51. Cassano, A.E.; Alfano, O.M. Reaction engineering of suspended solid heterogeneous photocatalytic reactors. *Catal. Today* **2000**, *58*, 167–197. [CrossRef]
52. Rafiq, A.; Ikram, M.; Ali, S.; Niaz, F.; Khan, M.; Khan, Q.; Maqbool, M. Photocatalytic Degradation of Dyes Using Semiconductor Photocatalysts to Clean Industrial Water Pollution. *J. Ind. Eng. Chem.* **2021**, *97*, 111–128. [CrossRef]
53. Gaya, U.I.; Abdullah, A.H. Heterogeneous photocatalytic degradation of organic contaminants over titanium dioxide: A review of fundamentals, progress and problems. *J. Photochem. Photobiol. C Photochem. Rev.* **2008**, *9*, 1–12. [CrossRef]
54. Hotze, E.M.; Phenrat, T.; Lowry, G.V. Nanoparticle Aggregation: Challenges to Understanding Transport and Reactivity in the Environment. *J. Environ. Qual.* **2010**, *39*, 1909–1924. [CrossRef] [PubMed]
55. Carrasco-Venegas, L.A.; Castañeda-Pérez, L.G.; Martínez-Hilario, D.G.; Medina-Collana, J.T.; Calderón-Cruz, J.C.; Gutiérrez-Cuba, C.; Cuba-Torre, H.R.; Núñez, A.P.; Herrera-Sánchez, S.E. Kinetics of Decolorization of Reactive Textile Dye via Heterogeneous Photocatalysis Using Titanium Dioxide. *Water* **2024**, *16*, 633. [CrossRef]
56. Kisch, H. Semiconductor Photocatalysis—Mechanistic and Synthetic Aspects. *Angew. Chem. Int. Ed.* **2013**, *52*, 812–847. [CrossRef] [PubMed]
57. Kumar, K.; Chowdhury, A. Use of Novel Nanostructured Photocatalysts for the Environmental Sustainability of Wastewater Treatments. In *Encyclopedia of Renewable and Sustainable Materials*; Elsevier: Amsterdam, The Netherlands, 2020; pp. 949–964. [CrossRef]
58. Gerischer, H.; Heller, A. The role of oxygen in photooxidation of organic molecules on semiconductor particles. *J. Phys. Chem.* **2002**, *95*, 5261–5267. [CrossRef]
59. Chowdhury, A.P.; Anantharaju, K.S.; Keshavamurthy, K.; Rokhum, S.L. Recent Advances in Efficient Photocatalytic Degradation Approaches for Azo Dyes. *J. Chem.* **2023**, *2023*, 9780955. [CrossRef]
60. Qian, R.; Zong, H.; Schneider, J.; Zhou, G.; Zhao, T.; Li, Y.; Yang, J.; Bahnemann, D.W.; Pan, J.H. Charge carrier trapping, recombination and transfer during TiO_2 photocatalysis: An overview. *Catal. Today* **2019**, *335*, 78–90. [CrossRef]
61. Kohtani, S.; Kawashima, A.; Miyabe, H. Reactivity of Trapped and Accumulated Electrons in Titanium Dioxide Photocatalysis. *Catalysts* **2017**, *7*, 303. [CrossRef]
62. Lettieri, S.; Pavone, M.; Fioravanti, A.; Amato, L.S.; Maddalena, P. Charge Carrier Processes and Optical Properties in TiO_2 and TiO_2-Based Heterojunction Photocatalysts: A Review. *Materials* **2021**, *14*, 1645. [CrossRef] [PubMed]
63. Chen, L.; Wang, Y.; Shao, H.; Mao, C.; Wu, M.; Xu, G. A comparison of the degradation of benzothiazole in the UV/H_2O_2 and UV/K_{2s2o8} systems: Degradation processes and degradation mechanisms. *Environ. Technol.* **2025**, *46*, 4774–4790. [CrossRef] [PubMed]
64. Chen, L.; Yin, W.; Shao, H.; Tu, M.; Ren, Y.; Mao, C.; Huo, Z.; Xu, G. The performance and pathway of benzothiazole degradation by electron beam irradiation. *Chemosphere* **2022**, *303*, 134964. [CrossRef] [PubMed]
65. Lai, W.W.-P.; Gu, F.-Y.; Tai, W.-L.; Tang, Z.-S. Degradation of benzotriazole and benzothiazole with the UV-activated peracetic acid process: Performance, mechanism and transformation pathway. *Environ. Sci. Water Res. Technol.* **2024**, *10*, 982–994. [CrossRef]
66. Lai, W.W.-P.; Lin, J.-C.; Li, M.-H. Degradation of benzothiazole by the UV/persulfate process: Degradation kinetics, mechanism and toxicity. *J. Photochem. Photobiol. A Chem.* **2023**, *436*, 114355. [CrossRef]